A generic binding pocket for small molecule I_{Ks} activators at the extracellular inter-subunit interface of KCNQ1 and KCNE1 channel complexes

Magnus Chan[1,*], Harutyun Sahakyan[3,4,*], Jodene Eldstrom[1,*], Daniel Sastre[1], Yundi Wang[1], Ying Dou[1], Marc Pourrier[1], Vitya Vardanyan[2,#], and David Fedida[1,#]

[1] Department of Anesthesiology, Pharmacology and Therapeutics, University of British Columbia, Vancouver, British Columbia, Canada, V6T1Z3.

[2] Molecular Neuroscience Group, Institute of Molecular Biology, NAS RA, 7 Hasratyan St. 0014 Yerevan, Armenia.

[3] Laboratory of Computational Modeling of Biological Processes, Institute of Molecular Biology of NAS RA, 0014, Yerevan, Armenia.

[4] Present Address: National Center for Biotechnology Information, National Library of Medicine, National Institutes of Health, Bethesda MD, USA.

[*]Contributed equally to the work in this paper.

[#]Email addresses for correspondence: david.fedida@ubc.ca and v_vardanyan@mb.sci.am

Keywords: ion channels, mefenamic acid, DIDS, I_{Ks}

Running Title: K^+ channel activator binding pocket

Dr. David Fedida
Life Sciences Centre, 2350 Health Sciences Mall, Room 2.301 Vancouver, British Columbia, Canada V6T 1Z3
Telephone: +1 (604) 822-5806, Email: david.fedida@ubc.ca

Abbreviations

I_{Ks}, delayed cardiac rectifier K^+ current; LQTS, long QT syndrome; DIDS, 4,4'-diisothiocyano-2,2'-stilbenedisulfonic acid; SITS, 4-acetamido-4'-isothiocyanatostilbene-2,2'-disulfonic acid; HMR1556, (3R,4S)-(+)-N-[3-hydroxy-2,2-dimethyl-6-(4,4,4-trifluorobutoxy) chroman-4-yl]-N-methylmethanesulfonamide; G-V, conductance-voltage relationship; *k*, slope factor; $V_{1/2}$, voltage at half-maximal activation; WT, wild type; ps-I_{Ks}, pseudo-KCNE1-KCNQ1; MD, molecular dynamics; MM, molecular mechanics; PBSA, Poisson-Boltzmann surface area; GBSA, generalized Born surface area.

Significance Statement

Combined, KCNQ1 and KCNE1 subunits generate the I_{Ks} current. Activating I_{Ks} has been identified as a promising therapeutic strategy to treat arrhythmogenesis resulting from delayed repolarization. In this study, we uncovered a common drug-induced binding site accessed by two structurally diverse I_{Ks} activators, mefenamic acid and DIDS. Located in the extracellular interface where KCNE1 interacts with KCNQ1, we propose that binding of drugs to this location impairs channel closing and leads to enhanced current activation. This is shown to be particularly beneficial at higher pulse rates and explains how such drugs may make an important contribution to the electrical repolarization reserve in the heart.

Abstract

The cardiac I_{Ks} ion channel comprises KCNQ1, calmodulin, and KCNE1 in a dodecameric complex which provides a repolarizing current reserve at higher heart rates and protects from arrhythmia syndromes that cause fainting and sudden death. Pharmacological activators of I_{Ks} are therefore of interest both scientifically and therapeutically for treatment of I_{Ks} loss-of-function disorders. One group of chemical activators are only active in the presence of the accessory KCNE1 subunit and here we investigate this phenomenon using molecular modeling techniques and mutagenesis scanning in mammalian cells. A generalized activator binding pocket is formed extracellularly by KCNE1, the domain-swapped S1 helices of one KCNQ1 subunit and the pore/turret region made up of two other KCNQ1 subunits. A few residues, including K41, A44 and Y46 in KCNE1, W323 in the KCNQ1 pore, and Y148 in the KCNQ1 S1 domain, appear critical for the binding of structurally diverse molecules, but in addition, molecular modeling studies suggest that induced fit by structurally different molecules underlies the generalized nature of the binding pocket. Activation of I_{Ks} is enhanced by stabilization of the KCNQ1-S1/KCNE1/pore complex, which ultimately slows deactivation of the current, and promotes outward current summation at higher pulse rates. Our results provide a mechanistic explanation of enhanced I_{Ks} currents by these activator compounds and provide a map for future design of more potent therapeutically useful molecules.

Introduction

Potassium ion (K^+) channel activators are important compounds in human health, as partial or complete loss of function of many K^+ channels may lead to inherited or acquired diseases that have significant morbidity and mortality. The delayed cardiac rectifier potassium current, I_{Ks}, plays an important role, especially at high heart rates, in the physiological shortening of the cardiac action potential (Sanguinetti et al., 1996). Unsurprisingly, mutations in both KCNQ1 (α-subunit) and KCNE1 (β-subunit), which when paired together give rise to the I_{Ks} current (Barhanin et al., 1996; Sanguinetti et al., 1996; Bendahhou et al., 2005), have been implicated in cardiac arrhythmia syndromes such as long QT syndrome (LQTS) and atrial fibrillation (Jervell and Lange-Nielsen, 1957; Wang et al., 1996; Chen et al., 2003; Eldstrom and Fedida, 2011; Olesen et al., 2014). With nearly all mutations seen in LQTS patients identified as loss-of-function and 50% of those loss-of-function mutations identified in the KCNQ1 subunit (Hedley et al., 2009; Ackerman et al., 2011), enhancing and activating I_{Ks} currents has long been suggested as a promising therapeutic approach for treating LQTS. It is a curiosity of I_{Ks} channels that the known activators fall into two general groupings: those that work best on the α-subunit, KCNQ1, alone, including zinc pyrithione, L-364,373, and one of the most studied activators, ML277 (Mattmann et al., 2012; Yu et al., 2013; Xu et al., 2015; Eldstrom et al., 2021); and those that work best in the presence of the auxiliary β-subunit, KCNE1, compounds like mefenamic acid and DIDS (4,4'-diisothiocyano-2,2'-stilbene disulfonic acid) (Abitbol et al., 1999; Wang et al., 2020).

Using cryo-EM, we recently visualized the binding of ML277 deep in the central core of KCNQ1 channels in a pocket lined inferiorly by the S4-S5 linker, laterally by the S5 and S6 helices of two separate subunits, and above by pore domain residues (Willegems et al., 2022). The location of the binding pocket and its structural inter-relationships help to explain the underlying mechanism of action of ML277, its specificity for KCNQ1, and the lack of efficacy due to steric hindrance in the presence of a β-subunit. However, it is known neither where activators of I_{Ks} bind that *require* the presence of the β-subunit, such as phenylboronic acid (Mruk and Kobertz, 2009), hexachlorophene, stilbenes such as DIDS and SITS (4-acetamido-4'-isothiocyanatostilbene-2,2'-disulfonic acid), and diclofenac acid derivatives such as mefenamic acid (Abitbol et al., 1999; Zheng et al., 2012; Wang et al., 2020), nor how they mediate their activator action. We have some clues for DIDS and mefenamic acid that their binding sites are not in the central channel core, as is the case for ML277, but depend on KCNE1 β-subunit residues at the extracellular surface of the channel, residues 39-43 in KCNE1 for DIDS (Abitbol et al., 1999) and K41 for mefenamic acid (Wang et al., 2020). Our recent cysteine scanning data revealed that although other extracellular KCNE1 residues in the same region to varying degrees impacted the effect of mefenamic acid, only the K41C mutation completely abolished mefenamic acid effect up to a concentration of 1 mM (Wang et al., 2020). Previous cross-linking studies have identified key interactions between this extracellular region of KCNE1 and the S1 and S6 transmembrane segments of KCNQ1 (Xu et al., 2008; Chung et al., 2009), suggesting that residues in either of these regions could also provide important clues to explain mefenamic acid's mechanism of action.

To further explore the dependence of residues in KCNE1 and those in adjacent KCNQ1 sites on binding of mefenamic acid to I_{Ks}, we first examined the role of K41C in preventing the drug effect. Docking in combination with molecular dynamics (MD) simulations of mefenamic acid binding to I_{Ks} followed by mutagenesis were used to map out critical KCNE1 and KCNQ1 residues. Further, we expanded on the idea that the stilbene, DIDS (Abitbol et al., 1999), which is structurally quite different from mefenamic acid, shares a common binding site. Our results

showed that both compounds bind in the same general region formed by elements of the pore and S6 domains of KCNQ1 and the near extracellular region of KCNE1, but depend on different critical residues for their binding stability. Exposure of the channel complex to either compound induces subtle structural changes that subsequently stabilize the conformation of the S1/outer pore/S6 of KCNQ1 and slow the I_{Ks} deactivation gating kinetics. The results suggest the existence of a common drug-induced binding site and a mechanism of action for small molecule I_{Ks} activators which is distinct from that of specific compounds that activate KCNQ1 alone.

Results

The mefenamic acid binding site on the KCNQ1/KCNE1 complex

Exposure of wild type I_{Ks} complexes (4:4 ratio; WT EQ) to 100 µM mefenamic acid transforms the slowly activating I_{Ks} current into one with an almost linear waveform and completely inhibits tail current decay at -40 mV (Figure 1A) (Abitbol et al., 1999; Unsöld et al., 2000; Wang et al., 2020). G-V relations obtained from peak initial tail currents show that 100 µM mefenamic acid hyperpolarizes the G-V ($\Delta V_{1/2}$ = -105.7 mV, Figure 1B, 1C) and decreases the slope (control k = 19.4 mV, Mef k = 41.3 mV, Table 1). We previously showed that introduction of a cysteine mutation at residue K41 in all four KCNE1 subunits (4:4 ratio of mutant K41C-KCNE1 to KCNQ1; K41C-EQ) itself had only a minor effect on the G-V, but prevented changes to currents and the G-V relationship on exposure to 100 µM or 1 mM mefenamic acid (Figure 1B, 1C and Table 1) (Wang et al., 2020). The data suggest that residue K41 in KCNE1 is critical to the action of mefenamic acid, but give no information why K41 is so important, and prompted us to question how this residue and other adjacent residues in KCNE1, and those nearby on KCNQ1 acted together to form a binding pocket for mefenamic acid.

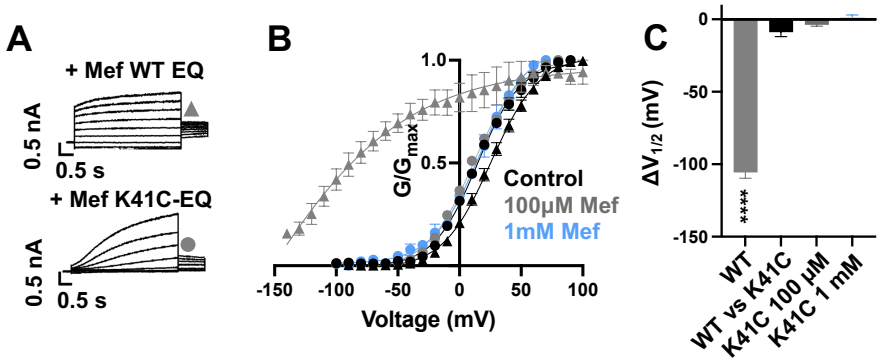

Figure 1. K41C-KCNE1 mutants prevent the agonist effect of mefenamic acid.
(A) Current traces of WT EQ (top) and K41C-EQ (bottom) in the presence of 100 µM mefenamic acid (Mef). A 4 s protocol was used with pulses from -150 mV or higher to +100 mV, in 10 mV steps, followed by a repolarization step to -40 mV for 1 s. Holding potential and interpulse interval were -80 mV and 15 s, respectively.
(B) G-V plots obtained from WT EQ tail currents (triangles) and K41C-EQ (circles) in the absence (control: black) and presence of Mef (100 µM: grey; 1 mM: light blue). Boltzmann fits were: WT EQ control (n = 6): $V_{1/2}$ = 25.4 mV, k = 19.4 mV; WT EQ 100 µM Mef (n = 3): $V_{1/2}$ = -80.3 mV, k = 41.3 mV; K41C-EQ control (n = 4): $V_{1/2}$ = 15.2 mV, k = 18.4 mV; K41C-EQ 100 µM Mef (n = 4): $V_{1/2}$ = 11.4 mV, k = 19.4 mV; and K41C-EQ 1 mM Mef (n = 3): $V_{1/2}$ = 16.7 mV, k = 19.8 mV.
(C) Summary plot of $V_{1/2}$ change ($\Delta V_{1/2}$) for WT EQ in the presence of 100 µM mefenamic acid, WT EQ vs K41C-EQ in control and K41C-EQ in the presence of 100 µM and 1 mM mefenamic acid. **** denotes a significant $\Delta V_{1/2}$ compared to control where $p<0.0001$.

Mefenamic acid binding site predicted by molecular modeling.

Initially, to visualise potential drug binding sites and understand how mutation of KCNE1 and KCNQ1 residues might prevent drug action, *in silico* experiments of drug docking with subsequent MD simulations were performed on a model of I_{Ks} channels. The I_{Ks} model was constructed based

on the recent cryo-EM structure of KCNQ1-KCNE3, which is thought to represent the activated-open state of the channel complex (Sun and MacKinnon, 2020). Taking into consideration the sequence similarity of KCNE1 and KCNE3 subunits in their transmembrane segments, it has been suggested that the main interface of these subunits with KCNQ1 is preserved in this region. Our initial data indicated that the extracellular residues of KCNE1 are involved in the action of I_{Ks} activators, so we constructed a model where external KCNE3 residues R53-Y58 were substituted with homologous KCNE1 residues, D39-A44 (Figure 2A). The resulting 4:4 I_{Ks} channel complex was termed pseudo-KCNE1-KCNQ1, ps-I_{Ks}, and Figure 2B shows the essential elements of the ps-I_{Ks} subunits which form extracellular interface of KCNQ1 and KCNE and served as a basis for drug docking and MD simulations. Details of the docking procedure are described in the Methods section and schematically summarized in Figure 2-figure supplement 1.

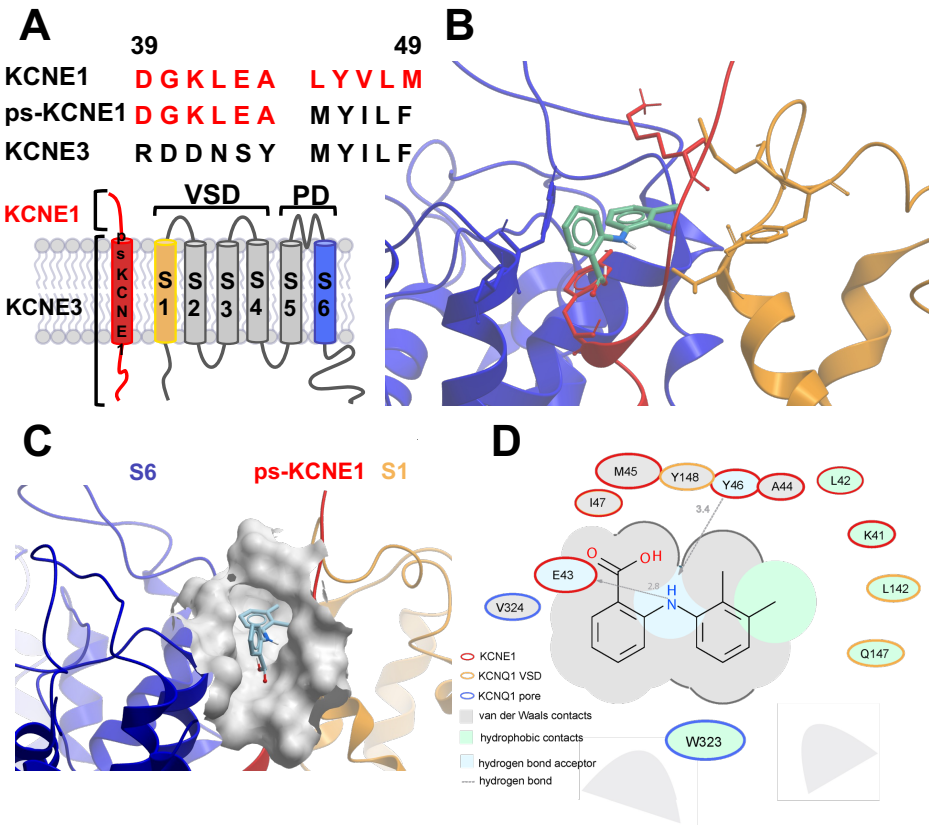

Figure 2. MD prediction of mefenamic acid binding site in the ps-I_{Ks} model.
(A) Pseudo-KCNE1 (ps-KCNE1) used to predict Mef binding site. Extracellular residues of KCNE1 (top), ps-KCNE1 (middle) and KCNE3 (bottom). Below, cartoon topology of the single transmembrane ps-KCNE1 β-subunit and the six transmembrane KCNQ1 α-subunit. S1-S4 transmembrane segments form the voltage sensor domain and S5-S6 form the pore domain.
(B) Predicted binding pose of Mef (green) in external region of the ps-I_{Ks} channel complex (side view). The residues of the pore domain are coloured in blue, ps-KCNE1 subunit in red, and the voltage-sensor domain of a neighbouring subunit is presented in yellow.
(C) Mef binding pocket in space-fill formed by external S1 (yellow) and S6 (blue) transmembrane domains of KCNQ1 and extracellular region of the ps-KCNE1 subunit (red).
(D) Ligand interaction map of Mef with ps-I_{Ks}. Size of residue ellipse is proportional to the strength of the contact. The distance between the residue label and ligand represents proximity. Grey parabolas represent accessible surface for large areas. The 2D diagram was generated by ICM pro software with cut-off values for hydrophobic contacts of 4.5 Å and hydrogen bond strength of 0.8. Further details in Methods.

170 Briefly, conformational sampling was performed on ps-I_{Ks} residues D39-A44, and conformations
171 showing the lowest free energy were selected for docking using a four-dimensional (4D) docking
172 approach to find the best binding pose of the ligand. A conformation with the best docking score
173 (Figure 2B) shows mefenamic acid binding to the pocket formed between extracellular KCNE1
174 residues, the external S6 transmembrane helix of one subunit, and the S1 transmembrane domain
175 of the neighboring subunit and the pore turret of a third subunit. The estimated volume of the
176 pocket in the mefenamic acid bound state is ~307 Å^3 with a hydrophobicity value of ~0.65
177 kcal/mol (Figure 2C). The free energy of the mefenamic acid-ps-I_{Ks} interaction estimated by the
178 MM/GBSA method from 300 ns MD simulations was -39.4 ± 0.3 kcal/mol (Figure 4A), while a
179 similar value of -31.8 ± 1.46 kcal/mol was calculated using the Poisson-Boltzmann surface area
180 (MM/PBSA) model. Mefenamic acid in this complex was stabilized by its hydrophobic and van
181 der Waals contacts with KCNQ1 and KCNE1 subunits as well as by two hydrogen bonds formed
182 between the drug and ps-KCNE1 residues Y46 and E43 (Figure 2D, Supplemental movie S1).

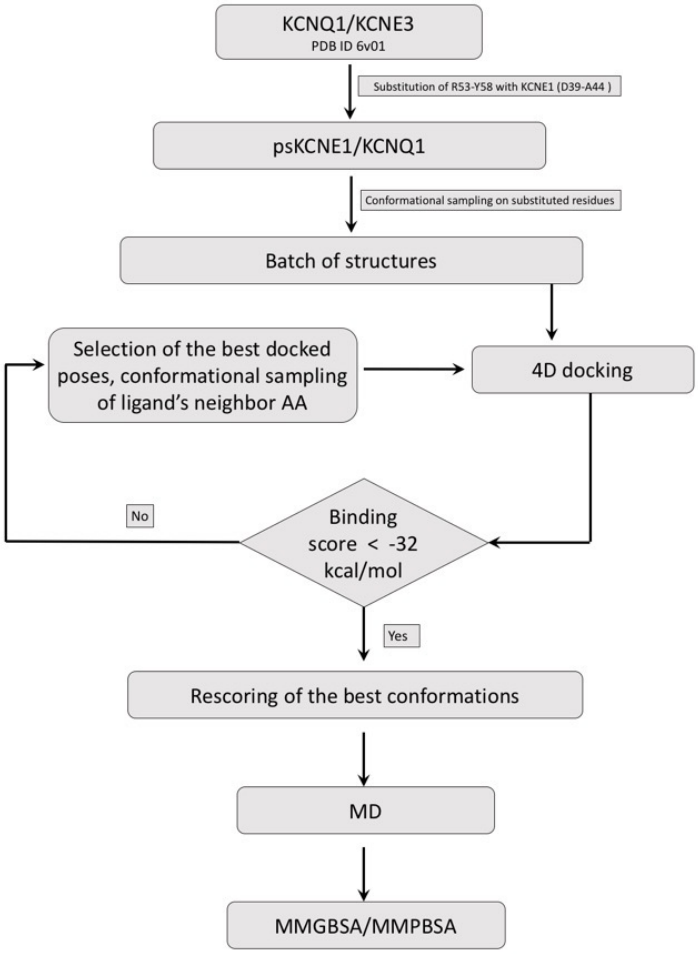

Figure 2-figure supplement 1. Drug docking and MD simulation workflow. (A) Schematic representation of the general workflow for construction of ps-I_{Ks}, Mef docking to the model ps-I_{Ks} channel complex and MD simulations (See Methods).

183
184 The energy decomposition per amino acid using MM/GBSA and MM/PBSA methods revealed
185 several residues in KCNQ1 and psKCNE1 with significant contributions to mefenamic acid
186 coordination (Figure 2D, Figure 2-figure supplement 2). As expected, these are the KCNE1

residues located at the external region of the auxiliary subunit – amino acids K41 to Y46. In addition, residues W323 and V324 located on the S6 helix as well as residues L142, Q147 and Y148 located on the S1 helix exhibited the lowest interaction free energy scores. We focused on functional validation of the KCNE1 residues K41, L42, E43, A44 and Y46, and KCNQ1 residues W323, V324, L142, Q147 and Y148 by mutation to cysteine, alanine and/or tryptophan, and examining the sensitivity of fully saturated EQ channel complexes to 100 µM mefenamic acid.

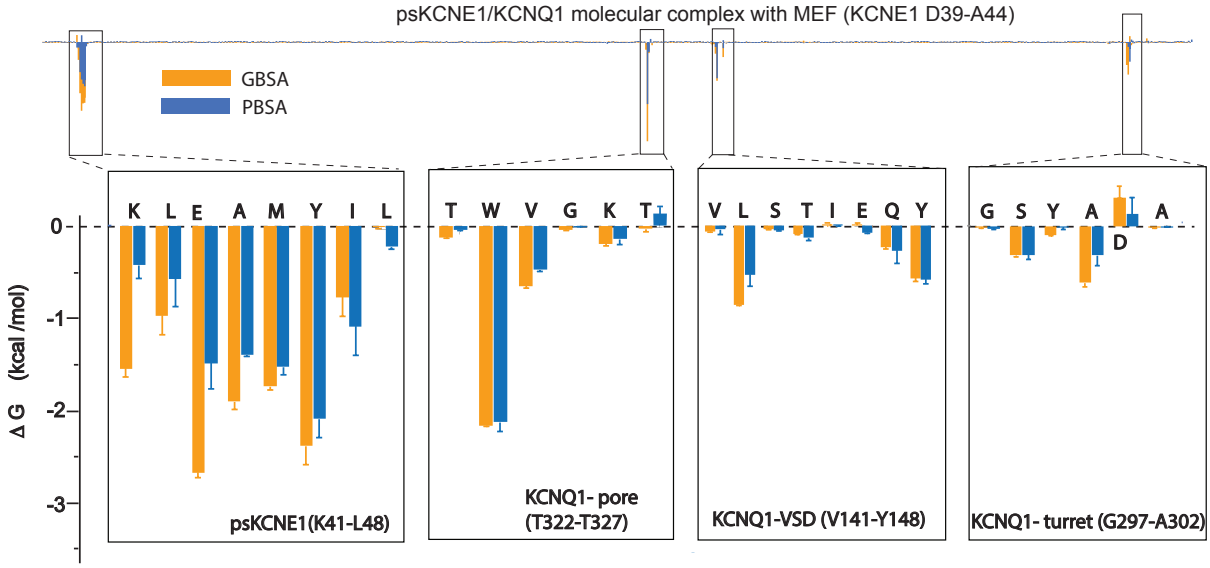

Figure 2-figure supplement 2. Energy decomposition per amino acid for mefenamic acid binding to ps-I_{Ks}. Poisson-Boltzmann Surface Area (PBSA; blue) and Generalized Born Surface Area (GBSA; orange) methods were used to estimate the interaction free energy contribution of each residue in the Mef-bound ps-I_{Ks} complex. The lowest interaction free energy for residues in ps-KCNE1 and selected KCNQ1 domains are shown as enlarged panels (n=3 for each point).

Mutational impact on EQ current changes induced by mefenamic acid.

The effect of mutations on the current waveform and tail current response to 100 µM mefenamic acid treatment was examined on I_{Ks} channels identified as: x-EQ-y where "x" denotes a KCNE1 mutation and "y" denotes a KCNQ1 mutation. In the absence of mefenamic acid (control), most mutations, with the exception of EQ-L142C (Figure 3-figure supplement 1), produced slowly activating currents with rapid tail current decay (Figure 3A).

In the presence of 100 µM mefenamic acid, the waveforms of WT EQ, S6 and pore mutations EQ-V324A, EQ-V324W, EQ-Q147C and EQ-Y148C were all transformed into ones with instantaneous current onset and slowed tail current decay (Figure 3A). Only the EQ-W323A waveform and tail current was largely unaffected by 100 µM mefenamic acid (like K41C-EQ, Figure 1). The EQ-W323C and A44C-EQ current waveforms were also unchanged by 100 µM mefenamic acid, but their tail current decay was slowed. We interpreted this to mean that mefenamic acid binds to EQ-W323C and A44C-EQ mutant open channels and slows closing, but that the drug-channel complex is less stable and mefenamic acid unbinds during the interpulse interval, which relieves drug action between pulses. The summary of the normalized response of the different mutants to mefenamic acid is shown in Figure 3D. G-V plots were obtained from the tail current amplitudes in the absence and presence of 100 µM mefenamic acid, and unlike WT EQ (Figure 1), minimal change in the shape and position of the EQ-W323A G-V plot was seen

after exposure to 100 µM mefenamic acid ($V_{1/2}$ shift of -14.1 mV compared with -105.7 mV seen in WT EQ (Figure 1, Figure 3B, 3E, and Table 1). For the W323C mutation, a less drastic decrease in size compared to alanine, the $V_{1/2}$ shift seen with 100 µM mefenamic acid increased (EQ-W323C $\Delta V_{1/2}$ = -26.5 mV), suggesting that the size of the W323 residue is important (Figure 3E and Table 1). However, when the neighboring V324 KCNQ1 residue was mutated to a smaller (alanine) or bulkier (tryptophan) residue they both showed the same response to mefenamic acid. Both the V324W and V324A mutations reduced $V_{1/2}$ shifts caused by 100 µM mefenamic acid to between -14 to -19 mV (Figure 3E and Table 1).

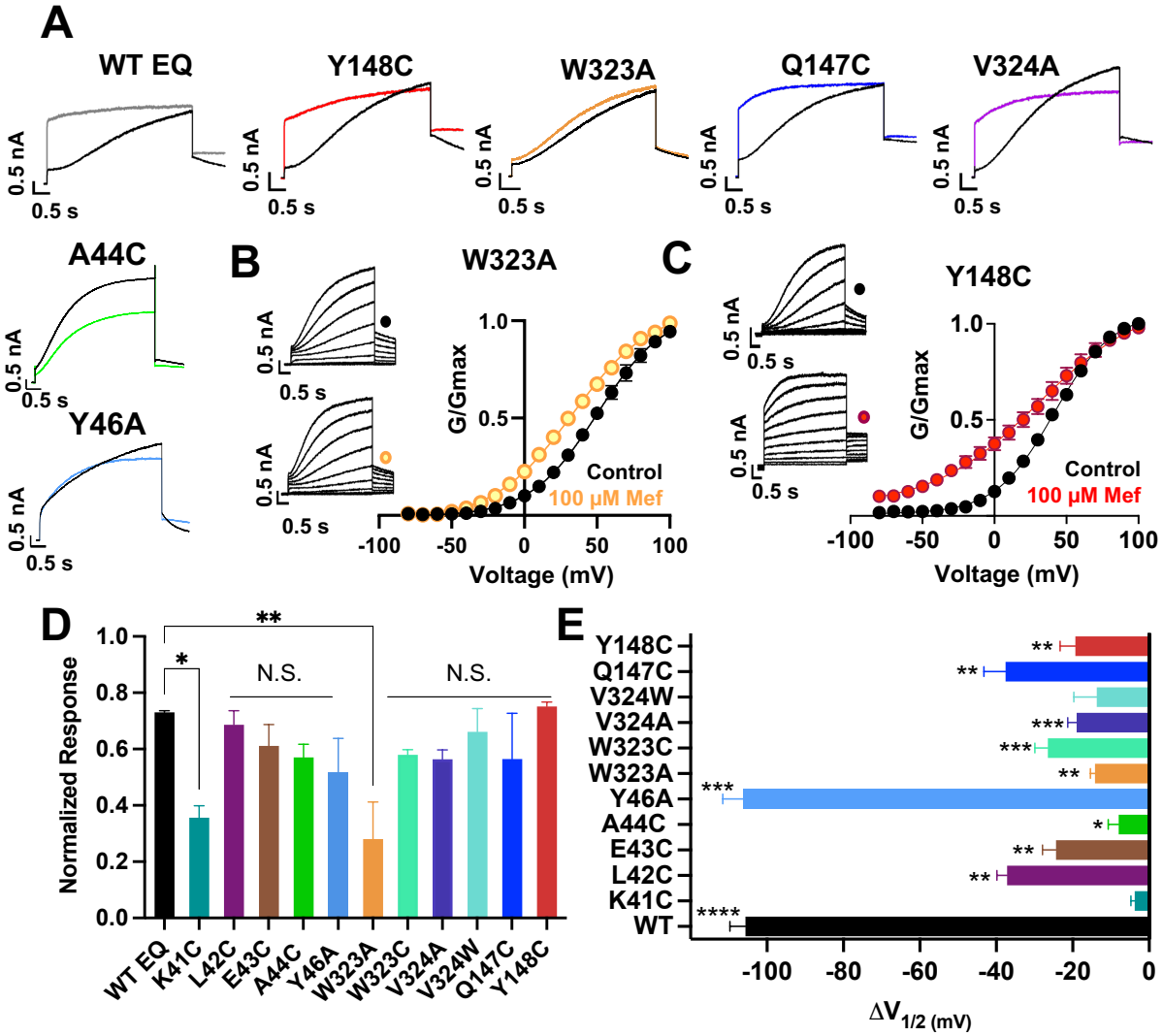

Figure 3. Current waveform and G-V changes induced by mefenamic acid in binding site mutants.
(A) Current traces from WT EQ and key residue mutants in control (black) and 100 µM Mef (colors).
(B) EQ-W323A and (C) EQ-Y148C current traces in control (top) and presence of 100 µM Mef (below). G-V plots in control (black) and presence of 100 µM Mef (colors). Boltzmann fits were: EQ-W323A control (n = 4): $V_{1/2}$ = 47.8 mV, k = 23.7 mV; EQ-W323A Mef (n = 3): $V_{1/2}$ = 33.7 mV, k = 28.5 mV; EQ-Y148C control (n = 4): $V_{1/2}$ = 36.8 mV, k = 20.3 mV; and EQ-Y148C Mef (n = 4): $V_{1/2}$ = 17.5 mV, k = 36.7 mV). Voltage steps were from -80 mV to +100 mV for 4 s, followed by a 1s repolarization to -40 mV. Interpulse interval was 15 s.
(D) Summary plot of the normalized response to 100 µM Mef (see methods). ** and * denote a significantly reduced response compared to WT EQ. N.S. denotes not significant.
(E) Plot of $V_{1/2}$ response ($\Delta V_{1/2}$) in drug for different mutants compared with WT. Significance of differences as stated in Methods. n-values for mutants in D and E are stated in Table 1.

Extracellular S1 residues identified in the MD simulations also proved to be important for mefenamic acid binding, although less so than W323 and K41 residues found in the KCNQ1 extracellular regions of the S6 segment and KCNE1, respectively. Compared to WT, EQ-Y148C reduced the $V_{1/2}$ shift after exposure to 100 µM mefenamic acid (EQ-Y148C $\Delta V_{1/2}$ = -19.3 mV) and lessened the slope of the G-V relationship (Figure 3C). The Q147C mutant on the other hand, only partially prevented the $V_{1/2}$ shift observed after mefenamic acid treatment (EQ-Q147C $\Delta V_{1/2}$ = -37.6 mV, Figure 3E).

Other KCNE1 residues located at the N-terminal limit of the KCNE1 transmembrane segment (L42, E43, A44, Y46) were also investigated. Unlike with K41C, but similarly to WT EQ, tail current decay was inhibited in the presence of 100 µM mefenamic acid in all of these mutants, reflected by the normalized response (Figure 3D). In addition, a reduced but statistically significant shift in $V_{1/2}$ was observed with 100 µM mefenamic acid compared to control in all mutants tested except K41C. (K41C $\Delta V_{1/2}$ = -3.8 mV; L42C $\Delta V_{1/2}$ = -37.1 mV; E43C $\Delta V_{1/2}$ = -24.4 mV; A44C $\Delta V_{1/2}$ = -9.7 mV; Figure 3D). Consistent with previous literature (Gofman et al., 2012; Wang et al., 2012; Kuenze et al., 2020), Y46C-EQ in control conditions produced a current with faster activation and a complex GV curve which made analysis and an assignment of slope and $V_{1/2}$ difficult, though a small left shift in the GV curve was visible (data not shown). In lieu of Y46C, G-V data from the Y46A-EQ mutant showed a potent effect of mefenamic acid, equivalent to that of WT with a $\Delta V_{1/2}$ = -106.2 mV (Figure 7-figure supplement 1). These results suggest that mutation of residues further away from the N-terminus of KCNE1 than K41 has diminishing effects on the activator action of mefenamic acid.

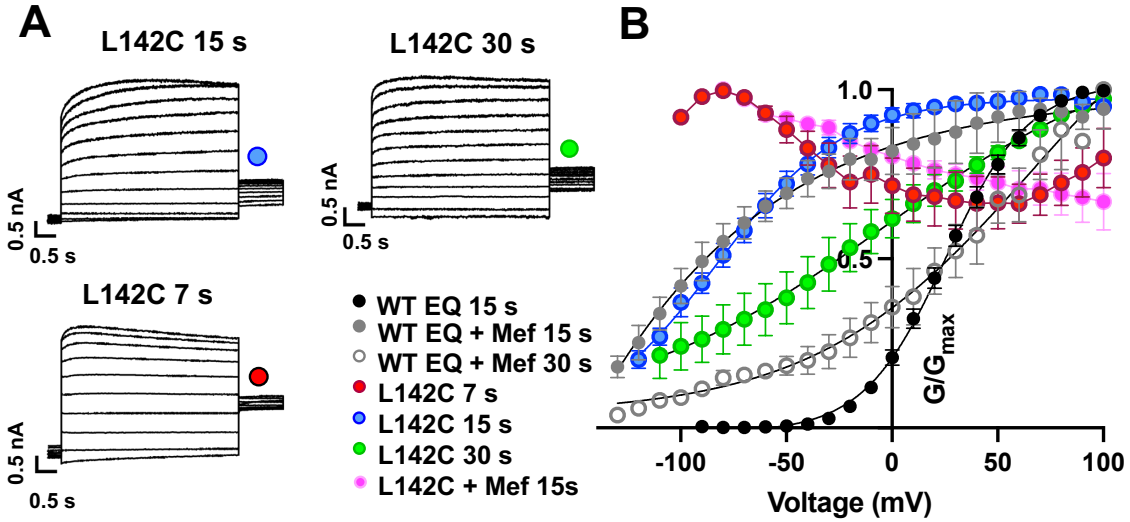

Figure 3-figure supplement 1. Augmented activation of EQ-L142C in the absence of mefenamic acid.
(A) EQ-L142C current traces in control solutions. Voltage steps were from -130 mV or higher in 10 mV steps to +100 mV for 4 s, followed by a repolarization step to -40 mV for 1 s. Holding potential was -80 mV. Interpulse interval was as indicated above, 15 s, 30 s and 7 s.
(B) G-V plot of WT EQ in control (interpulse interval 15 s: black) and in the presence of 100 µM Mef (interpulse interval 15 s: grey closed circle; 30 s: grey open circle) and EQ-L142C in control solutions (interpulse interval 7 s: red; 15 s: blue; 30 s: green). Boltzmann fits were: WT EQ 15 s control (n = 6): $V_{1/2}$ = 25.4 mV, k = 19.4 mV; WT EQ 15 s Mef (n = 3): $V_{1/2}$ = -80.3 mV, k = 41.3 mV; WT EQ 30 s Mef (n = 8); $V_{1/2}$ = 26.7 mV, k = 66.6 mV; EQ-L142C 15 s control (n = 6) $V_{1/2}$ = -80.3 mV, k = 30.0 mV; EQ-L142C 30 s control (n = 3) $V_{1/2}$ = -28.7 mV, k = 62.5. Due to the dramatic change in G-V plot shape, Boltzmann fits were not possible for EQ-L142C with an interpulse interval of 7 s. All mutations are forced saturated I_{Ks} channel complexes.

243 ***Augmented activation of EQ-L142C in the absence of mefenamic acid***
244 Unlike other mutations, the control EQ-L142C current waveform displayed an almost
245 instantaneous current onset, and tail currents showed no decay with our standard protocol (Figure
246 3-figure supplement 1A). As the control EQ-L142C current waveform qualitatively resembled WT
247 EQ currents in the presence of 100 µM mefenamic acid, G-V plots at different interpulse intervals
248 were compared. At the standard interval of 15 s, the EQ-L142C G-V plot (blue) closely overlapped
249 that of WT EQ in the presence of Mef (solid grey), and at a 30 s interpulse interval, the position
250 of the WT EQ + Mef (grey open circles) and EQ-L142C plots (green) both depolarized
251 significantly (Figure 3-figure supplement 1B). It appeared that the L142C mutation augmented
252 channel activation as much as 100 µM mefenamic acid on WT channels.
253 In addition, mefenamic acid made the EQ-L142C G-V plot voltage independent, overlapping with
254 the G-V obtained for EQ-L142C with a 7s interpulse interval (pink and red respectively, Figure 3-
255 figure supplement 1B). The data indicate that EQ-L142C is still responsive to mefenamic acid but
256 does so from a heightened state of activation (Table 2).
257
258 ***MD simulations of mutant ps-I_{Ks} channels exposed to mefenamic acid.***
259 To explore the role played by critical residues, *in silico* homologous mutations K41C and W323A
260 were introduced into the mefenamic acid-bound ps-I_{Ks} channel (Mef-ps-I_{Ks}) and the stability of the
261 Mef-mutant complexes was assessed during 300 ns MD simulations compared to the WT-Mef
262 complex. Remarkably, mefenamic acid detached from mutant K41C and W323A channels within
263 120-140 ns of MD simulations in all three independent runs (Supplemental movies S1- S3)
264 performed for each mutant. In contrast, mefenamic acid remained bound during the entire
265 simulation time to WT and Y46C-ps-I_{Ks} complexes (Supplemental movie S4). The last mutant was
266 tested as we could not determine the functional effect of mefenamic acid on this residue in
267 electrophysiological experiments. Mefenamic acid unbound from A44C- ps-I_{Ks} channel complexes
268 within 80, 100 and 110 ns during three different simulations, changing binding pose several times
269 before doing so.
270 A significantly *reduced* free interaction energy (ΔG) of ligand binding for all three mutant Mef-
271 ps-I_{Ks} complexes was observed compared to WT Mef-ps-I_{Ks} (Figure 4A, Table 3), and the small
272 but statistically significant change in free energy observed for the Y46C mutant complex indicates
273 that Y46 residue is not as important as K41 and W323 for mefenamic acid binding. Furthermore,
274 the flexibility of the external ps-KCNE1 protein residues of the mutants W323A and K41C ps-I_{Ks}
275 channels was analyzed by monitoring their average root mean square fluctuation (RMSF) during
276 the last 100 ns of simulations after the detachment of mefenamic acid from the molecular complex.
277 The RMSF values obtained from the two mutant channels were then compared to that of WT ps-
278 I_{Ks} channels where MD simulations of the same duration were conducted after removing the
279 mefenamic acid molecule from the complex (Figure 4B). The results indicate that W323A and
280 K41C mutations markedly increased the RMSF of D39-A44 ps-KCNE1 residues when compared
281 to the WT ps-I_{Ks} channel complex without mefenamic acid bound (Figure 4C, 4D). These results
282 suggest that the side chains of K41 and W323 residues normally stabilize the conformation of the
283 external region of KCNE1, so that mutation of these residues increases random motion and reduces
284 the ability of drugs like mefenamic acid to remain bound at this site.

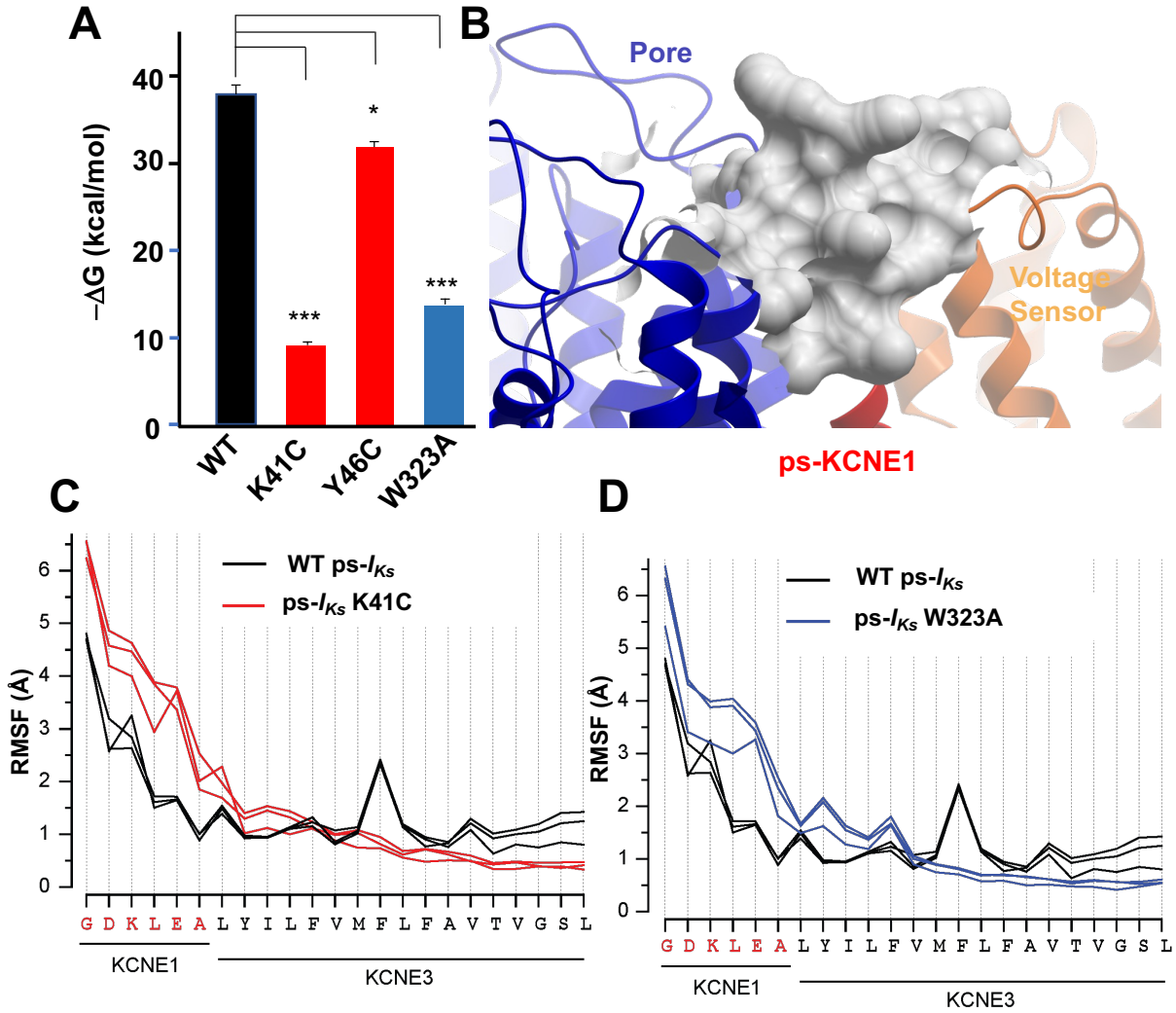

Figure 4. K41C, Y46C and W323A mutant Impact on mefenamic acid binding energy and flexibility of external KCNE1 residues.

(A) Average free interaction energy of Mef-bound ps-I_{Ks} complexes calculated according to MM/GBSA method from three independent MD simulation runs. For K41C and W323A mutations, calculations correspond to interval of simulations before the detachment of ligand from molecular complex. * and *** denote significant differences in average free interaction energy compared to WT.

(B) Surface representation of WT ps-I_{Ks} after removal of Mef. The pore is blue, ps-KCNE1 is red and the VSD of a neighbouring subunit is yellow.

(C-D) Root mean square fluctuations (RMSF) of ps-KCNE residues (Å) in the ps-I_{ks} complex during the last 100 ns of simulations. Three separate MD simulations shown for WT ps-I_{Ks} channel without Mef (black lines) and three for K41C (C, red) and W323A (D, blue) after ligand detachment. GROMACS software was used for RMSF analysis.

285

286 ***Mutational impact on I_{Ks} current changes induced by DIDS.***

287 To establish whether the binding pocket for mefenamic acid can be generalized to other I_{Ks}
288 activators, we also examined the binding of the structurally unrelated I_{Ks} activator, DIDS. Stilbenes
289 such as DIDS (Figure 5A) also activate I_{Ks} (Abitbol et al., 1999; Bollmann et al., 2020), and given
290 their molecular differences from fenamates, it is of interest to explore common structural and
291 dynamic features of their binding to the I_{Ks} channel complex. 100 μM DIDS had no effect on
292 endogenous currents in GFP-transfected tsA201 cells but treatment of WT EQ channels with 100

μM DIDS transformed the slowly activating waveform into one with faster onset (although not instantaneous like mefenamic acid) and inhibited tail current decay (Figure 5B). G-V plots were obtained from the tail amplitudes in the absence and presence of 100 μM DIDS (Figure 5C, 5D). The overall shape, slope, and $V_{1/2}$ of the WT EQ G-V relationship changed with 100 μM DIDS in the direction of increased activation ($\Delta V_{1/2}$ = -46.6 mV; Table 4; control k = 20.3 mV, DIDS k = 25.3 mV). However, the effects on WT EQ were less pronounced with DIDS than mefenamic acid at the 100 μM concentration.

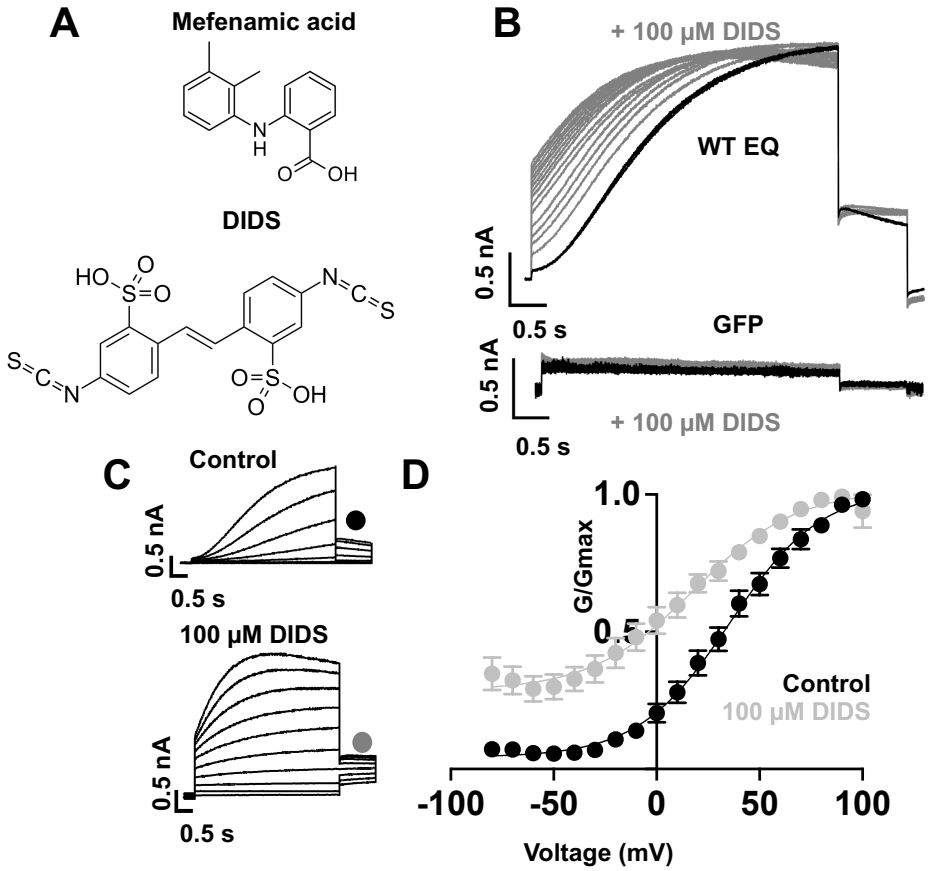

Figure 5. Effect of DIDS on I_{Ks}.
(A) Molecular structure of mefenamic acid and DIDS.
(B) WT EQ current in control (black) and exposed to 100 μM DIDS over time (grey). Pulses were from -80 to +60 mV every 15 s, and current traces are shown superimposed. Lower panel shows no effect on currents from GFP-only transfected cell exposed to 100 μM DIDS over time (grey).
(C) Current traces from WT EQ in control and presence of 100 μM DIDS as indicated. Pulses were from -80 to +100 mV for 4s, with a 1 s repolarization to -40 mV. Interpulse interval was 15 s.
(D) Corresponding G-V plot in control (black) and DIDS (grey) from data as shown in panel C. Boltzmann fits were: WT EQ control (n = 8): $V_{1/2}$ = 30.5 mV, k = 20.3 mV; WT EQ in the presence of DIDS (n = 5): $V_{1/2}$ = -16.1 mV, k = 25.3 mV.

The ps-I_{Ks} construct and docking procedures used previously to explore the binding site of mefenamic acid were used as a basis for DIDS docking and subsequent MD simulations. We found that DIDS also bound to a location formed between extracellular KCNE1 residues, the external S6 transmembrane helix of one subunit, the S1 transmembrane domain of the neighboring subunit, and the pore turret of the opposite subunit (Figure 6A). DIDS is stabilized by its hydrophobic and van der Waals contacts with KCNQ1 and KCNE1 subunits as well as by two hydrogen bonds formed between the drug and ps-KCNE1 residue L42 and KCNQ1 residue Q147. The energy decomposition per amino acid using MM/GBSA and MM/PBSA methods revealed several

residues in KCNQ1 and psKCNE1 with significant contributions to DIDS coordination (Figure 6B). Although residues identified as critical to mefenamic acid binding and action also generally appear to be important for DIDS, especially W323, K41 was noticeably not as critical to DIDS coordination whereas A44 and Y46 were more so.

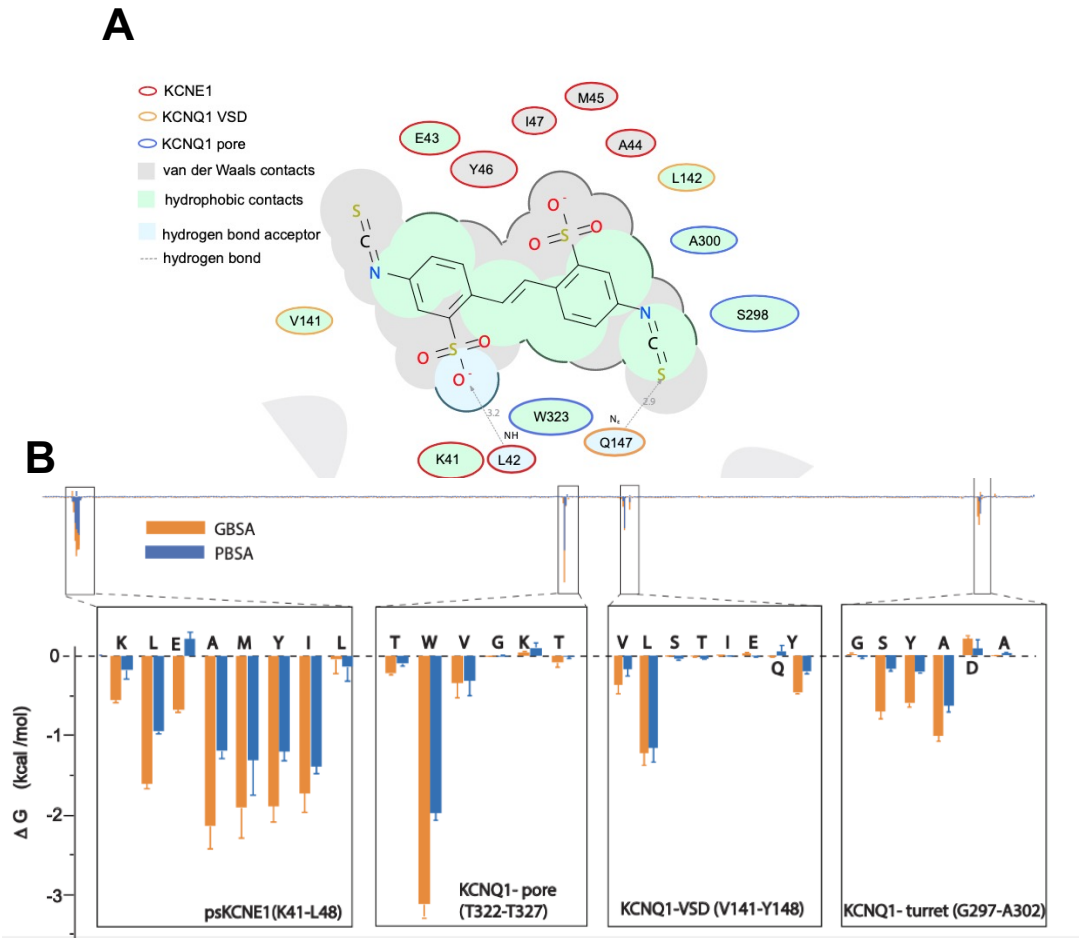

Figure 6. Ligand interaction and energy decomposition per amino acid for DIDS binding to ps-I_{ks}.
(A) Ligand interaction map of DIDS with ps-I_{Ks}. Size of residue ellipse is proportional to the strength of the contact. The distance between the residue label and ligand represents proximity. Grey parabolas represent accessible surface for large areas. The 2D diagram was generated by ICM pro software with a cut-off value for hydrophobic contacts 4.5 Å and hydrogen bond strength 0.8.
(B) Energy decomposition per amino acid for DIDS binding to ps-I_{Ks}. Generalized Born Surface Area (GBSA; orange) and Poisson-Boltzmann Surface Area (PBSA; blue) methods were used to estimate the interaction free energy contribution of each residue in the DIDS-bound ps-I_{Ks} complex. The lowest interaction free energy for residues in ps-KCNE1 and selected KCNQ1 domains are shown as enlarged panels (n=3 for each point).

Similar to mefenamic acid, DIDS stayed bound to WT ps-I_{Ks}, but detached from the W323A mutant during two of three runs, and from Y46C channels in one of three runs after 240 and 122 ns of simulation, respectively (Supplemental movies S5, S7). Interestingly, DIDS did not unbind from K41C mutant ps-I_{Ks} channels, even after 250 ns of simulation, although the binding pose did change in one run (Supplemental movie S6). Calculations of free interaction energy shown in Table 5 using both PBSA and GBSA methods are of mean values before the detachment of the drug if that occurred. If DIDS detachment did not occur during 250 ns MD runs, average free energy was calculated over the duration of the entire MD run for that construct. Only DIDS binding to W323A, and to Y46C in one simulation run, showed significantly lower free energy than DIDS

binding to WT, using both methodologies. The small change in free energy and more stable binding of DIDS to K41C suggest that this residue is not as important as W323 or Y46 for DIDS binding.

These model predictions were tested experimentally using fully saturated mutant I_{Ks} channel complexes, K41C-EQ, L42C-EQ, A44C-EQ, Y46A-EQ, EQ-W323A, EQ-L142C and EQ-Y148C (e.g. Figure 7A). Y46 was identified as an important residue for DIDS binding in MD simulations, but as before, the complexity of the GV curve and low functional expression of the Y46C construct led us to substitute Y46A for this mutation in electrophysiology experiments (Figure 7 and Figure 7-figure supplement 1).

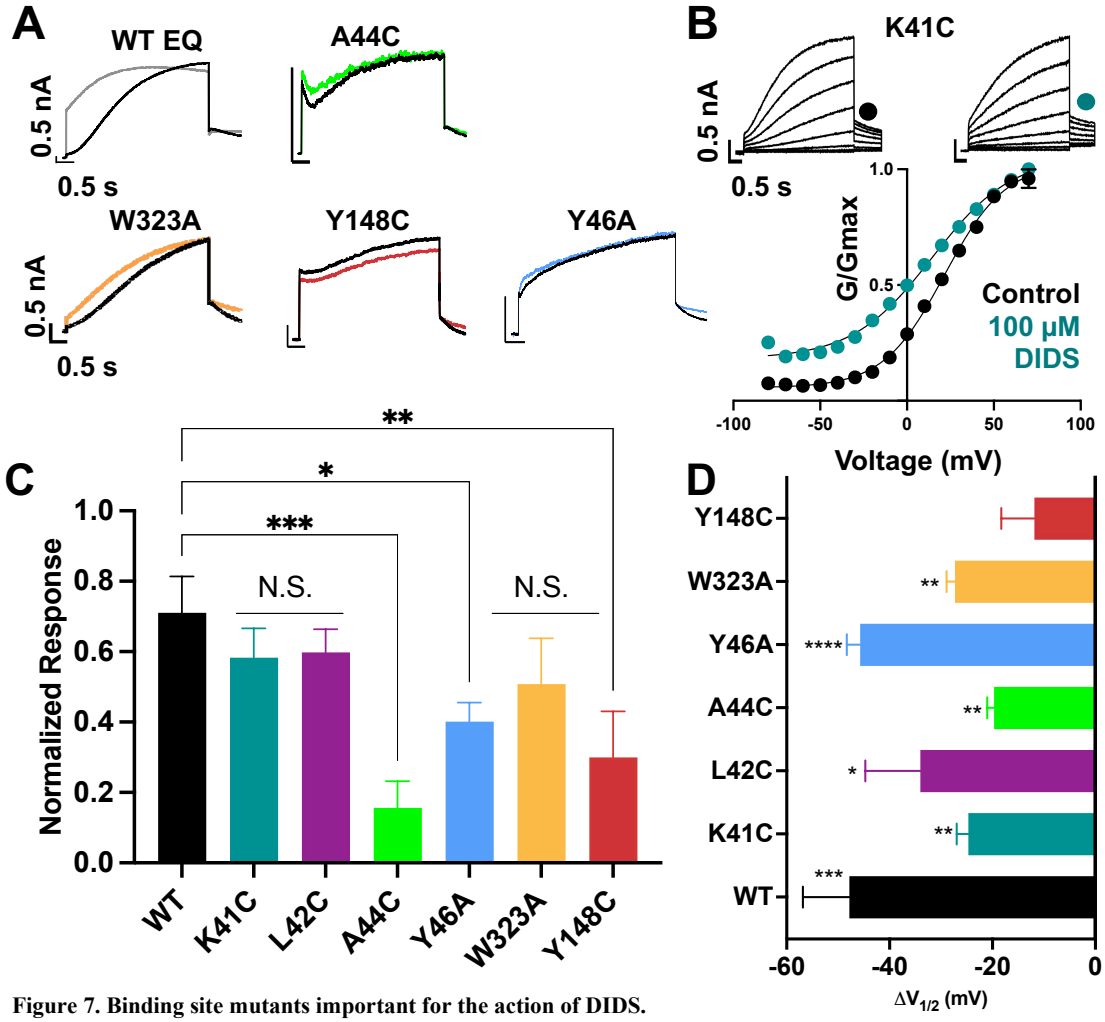

Figure 7. Binding site mutants important for the action of DIDS.
(A) Current traces from WT EQ and key mutants in the absence (control; black) and presence (colors) of 100 µM DIDS. All calibration bars denote 0.5 nA and 0.5 s.
(B) Data and G-V plots in control (black) and DIDS (teal). Boltzmann fits were: K41C-EQ control (n = 3): $V_{1/2}$ = 23.1 mV, k = 20.2 mV; K41C-EQ DIDS (n = 5): $V_{1/2}$ = -1.6 mV, k = 24.0 mV. Voltage steps from a holding potential of -80 mV to +70 mV for 4 s, followed by repolarization to -40 mV for 1 s. Interpulse interval was 15 s. All calibration bars denote 0.5 nA and 0.5 s.
(C) Summary plot of the normalized response to 100 µM DIDS. For calculation, see Methods.
(D) $V_{1/2}$ response ($\Delta V_{1/2}$) to 100 µM DIDS in different mutants compared to WT. Voltage protocol was as in panel B. n-values for mutants in C and D are stated in Table 4.

333 K41C-EQ G-V plots were obtained from peak tail current amplitudes in the absence and presence
334 (Figure 7B) of 100 µM DIDS. Unlike with mefenamic acid, but in agreement with the modeling,
335 K41C did not prevent the action of DIDS. Treatment of K41C-EQ with 100 µM DIDS
336 hyperpolarized the $V_{1/2}$ and changed the shape of the G-V relationship compared to control (Figure
337 7B, 7D, Table 4). The current waveform of K41C-EQ activated more quickly with less
338 sigmoidicity after treatment with DIDS, and tail current decay was slowed as indicated by the
339 normalized response (Figure 7B, 7C). As K41C-EQ remained responsive to DIDS, and L42C
340 responded similarly to K41C-EQ (for K41C-EQ, $\Delta V_{1/2}$ was -24.7 mV, and for L42C-EQ $\Delta V_{1/2}$ was
341 -34 mV), we hypothesized that DIDS binding to I_{Ks} channel complexes involved KCNE1 residues
342 closer to the transmembrane region as predicted by the ligand interaction map for DIDS (Figure
343 6A). In agreement with this idea, A44C showed little response to 100 µM DIDS both in term of
344 current waveform and tail current decay. The shift in $V_{1/2}$ was also reduced compared to WT-EQ
345 (A44C-EQ $\Delta V_{1/2}$ = -18.5 mV; WT EQ $\Delta V_{1/2}$ = -46.6mV, Figure 7C, D). In Y46A, the effect of
346 DIDS on the current waveform was greatly reduced as was slowing of tail current decay (Figure
347 7A, 7C). We could only estimate an activation $V_{1/2}$ for Y46A as the G-V curve was right shifted
348 to very positive potentials and non-saturating. Nevertheless, hyperpolarization of the $V_{1/2}$ (Figure
349 7D, Figure 7-figure supplement 1) in the presence of DIDS was observed, suggesting that unstable
350 and short-lived binding of the drug to the channel complex was sufficient to interfere with channel
351 gating.

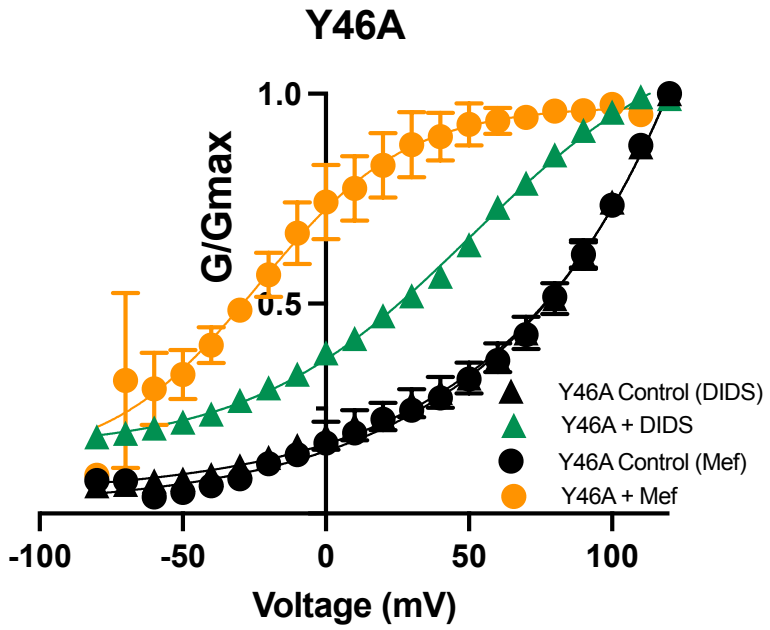

Figure 7-figure supplement 1: G-V plots for Y46A-EQ in the presence and absence of 100 mM mefenamic acid and DIDS.
G-V plots obtained from Y46A-EQ tail currents (circles and triangles) in the absence (control: black) and presence of Mef (100 µM: orange) and DIDS (100 µM: green).
Boltzmann fits were: Y46A-EQ control (n = 3): $V_{1/2}$ = 76.4 mV, k = 57.3 mV; Y46A-EQ Mef (n = 3): $V_{1/2}$ = -29.8 mV, k = 18.9 mV; Y46A-EQ control (n = 5): $V_{1/2}$ = 75.2 mV, k = 59.1 mV; Y46A-EQ DIDS (n = 5): $V_{1/2}$ = 25.8 mV, k = 39.2 mV.

352
353 The modeling studies (Figure 6) suggested that W323 remained a key residue for I_{Ks} activator
354 sensitivity, and in agreement with this, EQ-W323A was only partially responsive to DIDS. In EQ-
355 W323A, the tail current decay was affected but the slowly-activating current waveform was

356 preserved in the presence of DIDS, supporting the idea that the drug dissociates from the channel
357 complex between pulses (Figure 7A, 7C, Table 5). However, a significant shift in the $V_{1/2}$ remained
358 ($\Delta V_{1/2}$ = -27.3 mV; Figure 7D, Table 4). Comparable effects observed in EQ-W323A, A44C-EQ,
359 and Y46A-EQ are consistent with the idea that the DIDS binding pocket involves the N-terminal
360 end of S6 and the deeper extracellular surface of the KCNE1 transmembrane segment. In EQ-
361 Y148C, the $V_{1/2}$ and the shape of the G-V plot were not altered by 100 µM DIDS (Figure 7D,
362 Table 4), and tail current decay was not markedly slowed (Figure 7A, 7C). This result suggests
363 that unlike mefenamic acid, DIDS binding determinants extend to the S1 region of KCNQ1 and
364 that Y148 is an important contributor.
365 Notably, as with mefenamic acid, the L142C-EQ G-V plot became voltage-independent after
366 treatment with 100 µM DIDS (data not shown) and so it proved hyper-responsive to both of the
367 I_{Ks} activators, DIDS and mefenamic acid.
368
369
370 **Discussion**
371 Mefenamic acid, a nonsteroidal anti-inflammatory drug (NSAID), and the structurally distinct
372 stilbenes DIDS and SITS, among other compounds, have previously been identified by numerous
373 groups to enhance I_{Ks} currents in various expression systems including canine and guinea-pig
374 ventricular myocytes (Magyar et al., 2006; Toyoda et al., 2006) as well as heterologous expression
375 systems such as *Xenopus laevis* oocytes, CHO, COS-7, tsA201 and LM cells (Busch et al., 1994;
376 Abitbol et al., 1999; Unsöld et al., 2000; Toyoda et al., 2006; Wang et al., 2020). The extracellular
377 region of KCNE1 between residues 39-44 was found important in mediating the effect of DIDS
378 on I_{Ks} (Abitbol et al., 1999) and residue K41, located on the extracellular end of KCNE1, was
379 found to be critical in mediating mefenamic acid's activating effect on the fully saturated I_{Ks}
380 channel complex (Wang et al., 2020). Consistent with this idea, when all four WT KCNE1 subunits
381 are replaced with mutant K41C-KCNE1, mefenamic acid up to a concentration of 1 mM is largely
382 ineffective (Figure 1). Unlike in the WT complex, there is little change to the current waveform,
383 slope or $V_{1/2}$ of the G-V plot during activator exposure, suggesting that all the drug binding site(s)
384 on the channel complex are impaired, or that the mechanism of action is disabled, or that the
385 mutation causes a combination of these actions. In the present study, we analysed these activator
386 compound actions using molecular modeling approaches, and complementary mutational analysis.
387 Our data describe the formation of a drug binding pocket between the immediate extracellular
388 residues of KCNE1, S1 and pore residues of two KCNQ1 subunits, stabilized by the presence of
389 structurally different activator compounds. The effect of mutations that negate the activator
390 compound actions is to destabilize the binding pocket itself, reduce drug binding and limit activator
391 residency time on the channel complex.
392
393 ***Mefenamic acid binding site in I_{Ks}.***
394 Using data that suggested an extracellular binding site for mefenamic acid was at the KCNE1-
395 channel interface, MD simulations were used to explore drug-channel interactions further. The
396 drug binding pocket was defined as the extracellular space formed by KCNE1, the domain-
397 swapped S1 helices of one KCNQ1 subunit and the pore/turret region made up of two other
398 KCNQ1 subunits (Figure 2; Supplemental movie S1). Docking and molecular simulations
399 identified a binding site made up of several residues across all of these elements (Figure 2 and
400 Figure 2-figure supplement 2, Table 6). Mutagenesis revealed that most mutations impacted at
401 least one out of the three mefenamic acid effects: $V_{1/2}$ shift, GV-plot slope change, and current

402 waveform change related to slowed deactivation. However, only three of the mutants impacted all
403 of the mefenamic acid actions (Figure 3). These were W323A in KCNQ1, as well as K41C, and
404 A44C in KCNE1, which define key components of the binding pocket for mefenamic acid. That
405 W323 forms an important medial wall of the hydrophobic pocket to which mefenamic acid binds
406 is suggested by data from mutants in which the size of the side chain at this location is
407 systematically made smaller to cysteine then alanine, which results in diminished effectiveness of
408 the drug, particularly with alanine. This mutation resulted in the detachment of mefenamic acid as
409 well as lower interaction energy of drug-channel complexes during MD simulations (Figure 4A;
410 Supplemental movie S3) particularly loss of interaction strength with KCNE1 (Table 6). Likewise,
411 MD simulations revealed detachment of mefenamic acid and reduced interaction energy values for
412 K41C-Mef-I_{ks} complexes (Supplemental movie S2, Figure 4A) again accompanied by loss of
413 interaction strength with KCNE1 (Table 6). The drug also detached from the A44C complex,
414 another mutant with a reduced response in terms of changes in waveform, $V_{1/2}$ and slope. In
415 contrast, while the free interaction energy of the mutant Y46C channel was significantly decreased
416 in comparison to the WT channel complex (Figure 4A), detachment of mefenamic acid from the
417 mutant channel during 300 ns MD simulations was not observed, though S1 appears to pull away
418 from the pore (Supplemental movie S4). Comparison of energies at specific residues show a loss
419 of interaction with Q147 and Y148 in S1 with this mutant and a small shift towards the turret at
420 S298 and A300 (Figure 8A; Table 6). While we were not able to obtain good electrophysiological
421 data from Y46C, data from Y46A suggested that mefenamic acid still had potent actions on this
422 mutant. The combination of binding studies and electrophysiological data indicate that Y46 was
423 not as important for mefenamic acid binding and action as other KCNE1 N-terminal residues.
424
425 ***Common binding site for I_{Ks} activators, mefenamic acid and DIDS.***
426 Although it was suggested that DIDS and mefenamic acid have the same binding site (Abitbol et
427 al., 1999), the extent of overlap was unknown. Initially, we examined the effect of DIDS on WT
428 EQ. Consistent with previous studies (Abitbol et al., 1999; Bollmann et al., 2020) we confirmed
429 that 100 µM DIDS enhanced WT EQ activity (Figure 5B) with a $V_{1/2}$ shift of -46.6 mV and a
430 decrease in the slope of the G-V curve (Table 4). As most I_{Ks} activators are dependent on the
431 KCNQ1-KCNE1 stoichiometry, this more potent effect of DIDS seen in our study may be
432 explained by the higher dose we used and our KCNE1-KCNQ1 linked channel constructs, which
433 ensured fully KCNE1-saturated complexes. Furthermore, due to the large size and complex folds
434 found on the surface of oocytes, higher drug concentrations than those used for cultured cells are
435 often required in order to facilitate a similar effect in both expression systems (Kvist et al., 2011).
436 All previous studies utilized *Xenopus laevis* oocytes, whereas in this study transiently transfected
437 tsA201 cells were used.
438 *In silico* DIDS docking revealed that both mefenamic acid and DIDS bind to the same general
439 extracellular inter-subunit interface with some differences in key residues revealed by the
440 electrophysiology data. Mutation Y148 in KCNQ1 to a cysteine (Y148C) or Y46 in KCNE1 to an
441 alanine (Y46A) was found to reduce effects of 100 µM DIDS, particularly in the case of Y148C
442 (Figure 7). These data suggest that DIDS resides deeper in the binding pocket formed by KCNE1
443 residues and the KCNQ1 pore/S6, and so was less dependent on the side chain of K41 to retain the
444 activator on the channel complex (compare Movies S1 and S6). DIDS associated more strongly
445 with the pore of the Y148C mutant, particularly with V324 and T327, and less across the
446 KCNE1/3, S1 and turret regions (Table 6). The Y46C mutation resulted in shifts away from
447 KCNE1/3 and towards the S1 domain (T144, E146 and Q147). In the case of A44C and DIDS, the

448 changes were more subtle, with stronger interactions moving from central residues in KCNE1
449 (K41, L42 and E43) and S1 (V141 and L142; coloured grey in Figure 8B) to more peripheral
450 residues (I145, E146 and Q147) and lower in the KCNE TMD (A44 and M45; coloured magenta
451 in Figure 8B).

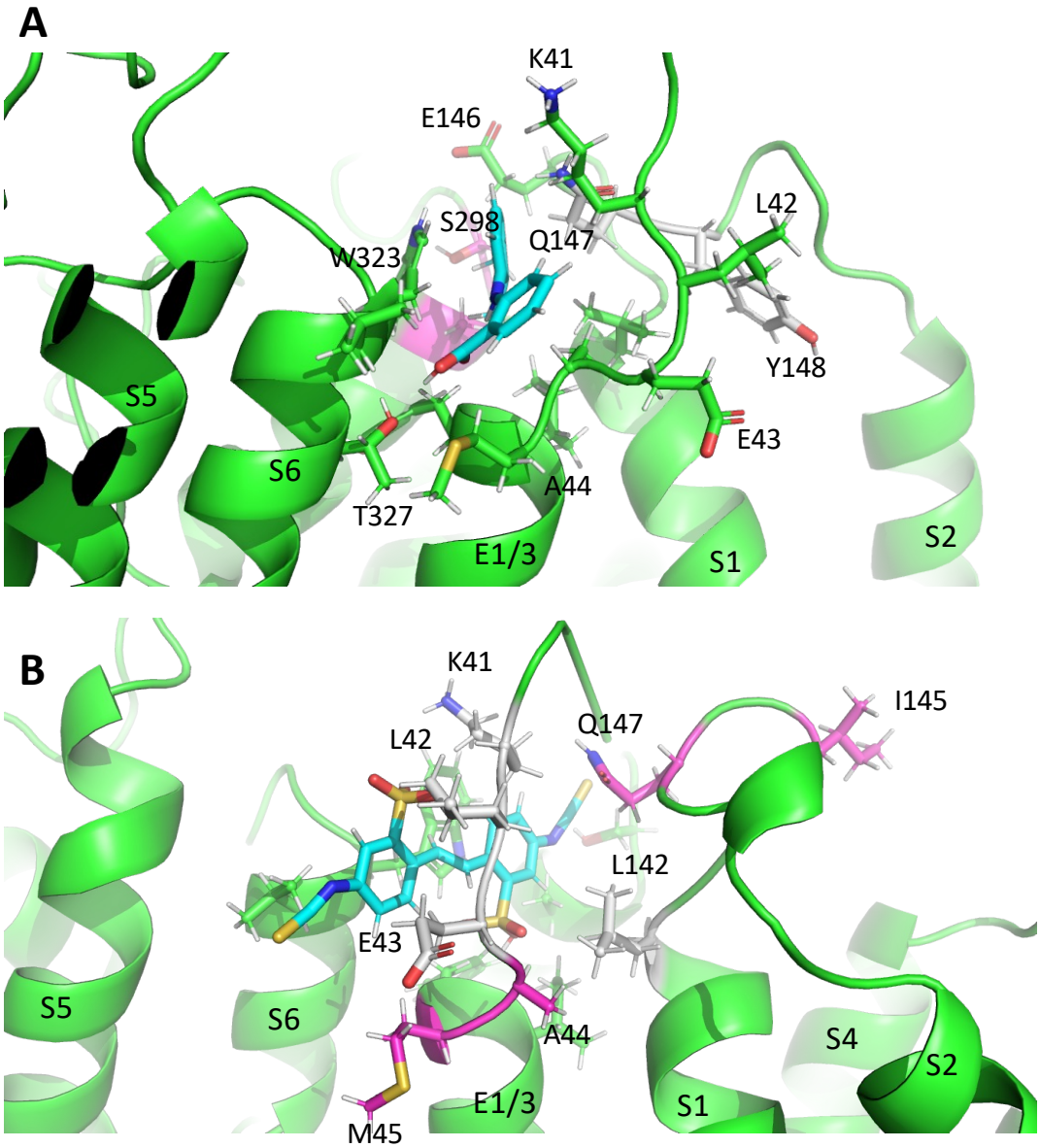

Figure 8. Subtle differences in activator binding to Y46C- and A44C-ps-IKs mutant channels. (A) Mefenamic acid bound to the WT ps-IKs channel. Residues that are part of the binding site are shown in stick format colored green, except those residues that were important in the WT channel that had reduced ΔG in Y46C (in grey). Residues that had slight increases in ΔG values in Y46C are shown in magenta (S298, A300). Mefenamic acid is in cyan.
(B) DIDS bound to the WT ps-IKs channel. Residues that are part of the binding site are shown in stick format colored green except those residues that were important in the WT channel that had reduced ΔG in the A44C mutant (in grey). Residues that had slight increases in ΔG values in A44C are shown in magenta. DIDS is in cyan. Images were made with the PyMOL Molecular Graphics System, Version 2.0 Schrödinger, LLC.

452

453 ***Proposed mechanism of action for mefenamic acid and DIDS.***
454 Molecular modeling and docking revealed that mefenamic acid and DIDS induce conformational
455 changes in the channel upon binding, to shape a binding pocket formed by residues from the
456 external S1 domain, KCNE1 and the pore domain of I_{Ks} (Figure 2C, Supplemental movies S1, S5).
457 This cryptic binding pocket is not detectable in the absence of the drug (Figure 4B), which suggests
458 that it has been induced in a similar manner to previous reports of toxin interactions with KcsA-
459 Kv1.3 that induce conformational changes in both the toxin and the channel structure to generate
460 a high-affinity binding site (Lange et al., 2006; Zachariae et al., 2008). Given the high modeled
461 binding energy of the channel-drug activated state complexes, ~-39 kcal/mol for mefenamic acid
462 and ~-35 kcal/mol for DIDS, but the relatively low affinities, given the micromolar concentrations
463 required experimentally, we can imagine a dynamic complex where mefenamic acid and DIDS
464 bind/unbind from I_{Ks} at high frequency. Slowed deactivation may therefore be the result of these
465 rapid binding/unbinding interactions slowing the dissociation of the S1/KCNE1/pore domain/drug
466 complex by either providing steric hindrance to dissociation or by stabilizing the activated
467 complex. MD simulations suggest the latter is most likely the case. Our data indicate that mutation
468 of residue W323 to an alanine would not only destabilize the external S1/KCNE1/pore domain
469 interface (Figure 4D, Table 1) but also eliminate direct hydrophobic contacts which normally occur
470 between the W323 side chain and mefenamic acid, thus facilitating drug dissociation (Figure 2D,
471 Supplemental movie S3).
472 A reduced interaction with S1 could also conceivably curtail the ability of I_{Ks} activators to slow
473 dissociation of the activated complex and restore faster deactivation rates such that there is no
474 longer an enhanced step current in the presence of the drug, as seen in mutants K41C and A44C
475 for mefenamic acid (Figure 1A and 3A) and A44C, Y46A, W323A and Y148C for DIDS (Figure
476 7A). Similarly, electrostatic interactions of residue K41, which acts as a lid for the binding pocket
477 for mefenamic acid (Supplemental movie S2), could help stabilize the protein-protein interface at
478 the external region of the channel complex. Mutation of residue K41 to a cysteine may prevent
479 stable I_{Ks} activator binding to the channel by increasing the fluctuations of the external KCNE1
480 region (Figure 4C) and by reducing van der Waals contacts with the drug (Figure 2D). In
481 simulations, mefenamic acid was seen dissociating from mutant K41C, A44C, and W323A
482 channel complexes, and this explains why the electrophysiological effects of I_{Ks} activators were
483 prevented by the mutational substitutions at these locations (Supplemental movies S2, S3). Shifts
484 in, and particularly reductions in KCNE1/3 association for both drugs (Table 6) that lead to loss
485 of efficacy suggest that it is the interactions with KCNE1 and S1 that are key to maintaining the
486 activated state. This is similar to the proposal for tight interactions between S1 and KCNE3 in
487 maintaining constitutive activity in KCNE3-associated channels (Kasuya and Nakajo, 2022).
488
489 In close proximity to this drug-binding pocket are known gain-of function mutations in S1, S140G
490 and V141M, which have previously been reported to slow deactivation in the presence of KCNE1
491 (El Harchi et al., 2010; Peng et al., 2017). As their current waveforms are qualitatively similar to
492 those seen after exposure of WT EQ to I_{Ks} activators, we propose that the same mechanism may
493 underlie the effects of mefenamic acid, DIDS and these I_{Ks} S1 mutations. In addition, we find that
494 mutation of the neighboring residue, L142, also produces current waveforms and G-V plots which
495 mirror those seen when WT EQ is treated with 100 μM mefenamic acid (Figure 3-figure
496 supplement 1) or DIDS. In the cryo-EM structure of KCNQ1-KCNE3 (Sun and MacKinnon,
497 2020), residue L142 interacts with KCNE3, whereas V141 interacts with both KCNE3 and the
498 pore domain. This suggests that both the V141M and L142C mutations could directly alter the

interaction of the S1 domain with the pore and/or the position or movement of KCNE1. The co-evolved interface between the extracellular end of S1 and the pore domain is thought to be important for bracing the VSD, to allow efficient force transmission to the pore (Lee et al., 2009), but can also impact permeation, as the S140G and V141M mutations also enhance rubidium permeation through I_{Ks} complexes (Peng et al., 2017). The importance of this S1-pore coupling to channel function is supported by mutational analyses of S1 residues (Chen et al., 2003; Hong et al., 2005; Wang et al., 2011; Campbell et al., 2013) as well as the L142C mutation examined in this study (Figure 3-figure supplement 1), which all display current waveforms with instantaneous onset. Incidentally, A300, a residue in the pore region of KCNQ1, which also interacts with both mefenamic acid and DIDS in MD simulations (Figure 2-figure supplement 2, Figure 6), has also been implicated in the same gain-of-function cleft as S140G and V141M (Smith et al., 2007). The V300T mutant has an ~-20 mV shift in $V_{1/2}$ of activation and faster rates of activation (Bianchi et al., 2000), once again showing how a mutation can mirror the effects of the two activators studied here.

Conclusion

Binding of mefenamic acid and DIDS to the extracellular end of KCNE1 and the KCNQ1 S6 and S1 helices is facilitated by a number of key residues. Residue K41 acts as a "lid" holding mefenamic acid in place, while residue W323 impacts the size of the binding pocket. Size reduction mutations of either residue destabilize mefenamic acid binding and ultimately lead to drug detachment from the channel complex. This explains why, when all four I_{Ks} subunits are mutated, as in the case of K41C-EQ, EQ-W323A and A44C-EQ, little to no effect of the drug is seen. The larger drug, DIDS, interacts with many of the same residues but those deeper in the pocket appear more important than for mefenamic acid. Furthermore, the qualitative similarities between the S1 mutant channel, EQ-L142C and WT EQ in the presence of 100 μM mefenamic acid suggest that I_{Ks} activators most likely cause their effects by modulating interactions between the S1 helix, pore turret, KCNE1 and the S6 helix. Upon binding, both DIDS and mefenamic acid induce conformational changes in an occult binding pocket and stabilize the S1/KCNE1/pore complex, which ultimately slows deactivation. The results indicate that this extracellular inter-subunit interface forms a generalized binding site which different drugs can access and through which induce common effects on channel activation and deactivation. The presence of such a binding site and the variable nature of I_{Ks} complex composition may serve as starting points for future drug development projects targeted at discovering therapeutically-useful I_{Ks} agonists.

534 **Materials and Methods**

535 ***Drug docking and Molecular Dynamic simulations***

536 A model of the I_{Ks} channel complex – termed pseudo-KCNE1-KCNQ1 (ps-I_{Ks}) – was created based
537 on the cryogenic electron microscopy (cryo-EM) structure of KCNQ1-KCNE3 (PDB ID: 6v01)
538 (Sun and MacKinnon, 2020). In this structure, the extracellular residues of KCNE3, R53-Y58,
539 were substituted with homologous KCNE1 residues D39-A44. Conformational sampling was then
540 performed for substituted residues and the lowest free energy conformations were selected for
541 subsequent docking experiments applying a four-dimensional (4D) docking approach which
542 accounts for the flexibility of the receptor site configuration (Bottegoni et al., 2009). A receptor
543 ensemble was then created via another round of conformational sampling for the external part of
544 ps-KCNE1 and its KCNQ1 neighborhood (8 Å cut-off distance) and generated conformations were
545 used for a new docking iteration. A ligand-channel conformation with the lowest free energy was
546 chosen from final docking iterations. The docking and conformational sampling experiments as
547 well as *in silico* mutations described in this study were performed with ICM-pro 3.8 software
548 (Molsoft LLC, San Diego) (Neves et al., 2012). The coordinates of selected mefenamic acid-bound
549 ps-I_{Ks} channel complexes with the lowest free energy were then used for MD. To keep the voltage-
550 sensing domain (VSD) in its upstate conformation, we restrained the PIP2 molecule in its
551 crystallographic position during MD simulations. Simulations were performed in a water
552 environment with AMBER20 using a ff14SB force field for proteins and GAFF/AM1-BCC
553 scheme for the ligand parameterization and calculation of the atomic point charges (Jakalian et al.,
554 2002; Case et al., 2005; Maier et al., 2015). The complex was solvated with TIP3P water models
555 and Na^+/Cl^- at 100 mM concentration. The system was minimized and equilibrated during 10 ns.
556 In all simulations described in this study the Langevin thermostat was set with collision frequency
557 2 ps^{-1}, the reference temperature 310 degrees K, and Monte Carlo barostat with reference pressure
558 at 1 bar (Oliver et al., 1997; Wu et al., 2016). The long-range electrostatic interactions with a cut-
559 off at 10 Å were treated with the Particle Mesh Ewald (PME) method. Bonds involving only
560 hydrogens were constrained with the SHAKE algorithm and a 2 fs integration time step was used.
561 The 2D diagrams in Figures 2 and 6 were generated by ICM pro software. Cut-off values are as
562 follows: hydrophobic contacts 4.5 Å and hydrogen bond strength 0.8. Hydrogen bond strength is
563 a unitless parameter for H-bond calculation in ICM-pro and lower values identify weaker hydrogen
564 bonds. The values do not represent H-bond energy. The MM/PBSA and MM/GBSA methods were
565 used to calculate the free energy of binding as described previously (Miller et al., 2012) after
566 collection of 1000 snapshots for each run. A schematic representation of the general workflow for
567 ps- I_{Ks} model construction, drug docking and MD simulations can be found in Figure 2-figure
568 supplement 1.
569

570 ***Reagents and solutions***

571 DIDS (Sigma-Aldrich, Mississauga, ON, Canada) was prepared as a 50 mM stock solution
572 dissolved in 100% dimethyl sulfoxide. Stock DIDS solution was diluted in control whole-cell bath
573 solution to obtain a final DIDS concentration of 100 µM which was perfused onto mammalian
574 cells for whole-cell experiments. All other reagents and solutions were prepared as described
575 (Wang et al., 2020). Mefenamic acid (Tocris Bioscience, Oakville, ON, Canada) was used at
576 concentrations of 100 µM and 1 mM. To block I_{Ks}, the specific I_{Ks} inhibitor HMR1556 (Tocris
577 Bioscience, Oakville, ON, Canada) was used at a concentration of 0.3-1 µM.
578

579 ***Molecular biology, cell culture and whole cell patch clamp***

580 tsA201 transformed human embryonic kidney 293 cells were first cultured, then plated for whole-
581 cell experiments and, finally, transfected with Lipofectamine2000 (Murray et al., 2016; Westhoff
582 et al., 2019; Wang et al., 2020). All mutations were first generated using site-directed mutagenesis
583 and Pfu turbo, then sequence confirmed. Whole-cell experiments were conducted 24-48 h post
584 transfection. For wildtype (WT) EQ and mutant x-EQ-Y (where "x" denotes a KCNE1 mutation
585 and "y" denotes a KCNQ1 mutation; for example, K41C-EQ, EQ-W323A), cells were transfected
586 with a linked KCNE1 and KCNQ1 cDNA (2-3 µg was used) which assembles as a fully saturated
587 4:4 ratio of KCNE1 to KCNQ1. All constructs were also co-transfected with 0.8 µg of GFP to
588 allow transfected cells to be identified. Data were obtained using an Axopatch 200B amplifier,
589 Digidata 1440A digitizer and pCLAMP 11 software (Molecular Devices, LLC, San Jose, CA).
590
591 ***Data analysis***
592 Conductance-voltage (G-V) relationships were obtained from the normalized peak of the initial
593 tail current (G/Gmax) and plotted against the corresponding voltage. G-V plots were fitted with a
594 Boltzmann sigmoid equation to obtain the voltage at half-maximal activation ($V_{1/2}$) and slope (*k*)
595 values (Tables 1 to 3). For each EQ mutant, the change in activation $V_{1/2}$ ($\Delta V_{1/2}$=$V_{1/2}$ in the
596 presence of drug-$V_{1/2}$ control) was also determined (Figures 3E and 7E). In some cases, the foot
597 of the G-V curve did not reach 0 (essentially in the presence of drug) and as a result, the $V_{1/2}$ was
598 read directly from the plots. Slowing of tail current decay was used as a measure of mefenamic
599 acid and DIDS impact on WT and mutated EQ channel complexes. Specifically, the peak to end
600 difference currents were calculated by subtracting the minimum amplitude of the deactivating
601 current from the peak amplitude of the deactivating current. The difference current in mefenamic
602 acid or DIDS was normalized to the maximum control (in the absence of drug) difference current
603 and subtracted from 1.0 to obtain the normalized response (Figures 3D and 7C).

604 GraphPad Prism 9 (GraphPad Software, San Diego, CA) was used to analyze all the data. Where
605 applicable, unpaired t-test or one-way ANOVA followed by the Fisher's least significant
606 difference (LSD) test was used to determine statistical significance. In all figures ****, ***, **, *
607 denotes a significance where $p<0.0001$, $p<0.001$, $p<0.01$ and $p<0.05$, respectively. All data in the
608 figures and tables are shown as mean ± SD or SEM. Bar graphs showing mean $\Delta V_{1/2}$ (Figures 3E
609 and 7D) were generated by calculating changes in $V_{1/2}$ induced by drug treatment vs. control in
610 separate cells. $\Delta V_{1/2}$ values reported in the Results were calculated from the mean $V_{1/2}$ values
611 shown in Tables 1 and 3.

Acknowledgements

We thank Fariba Ataei for her assistance in cell culture and for making mutants.

Authorship Contributions

Participated in research design:
Jodene Eldstrom, David Fedida, Vitya Vardanian, Harutyun Sahakyan, Magnus Chan, Marc Pourrier, Yundi Wang

Conducted experiments:
Magnus Chan, Harutyun Sahakyan, Daniel Sastre, Marc Pourrier, Jodene Eldstrom, Yundi Wang, Ying Dou, David Fedida

Performed data analysis:
Magnus Chan, Jodene Eldstrom, Harutyun Sahakyan, Yundi Wang

Wrote or contributed to the writing of the manuscript:
David Fedida, Harutyun Sahakyan, Jodene Eldstrom, Magnus Chan, Marc Pourrier, Yundi Wang, Vitya Vardanian

References

Abitbol I, Peretz A, Lerche C, Busch AE, and Attali B (1999) Stilbenes and fenamates rescue the loss of I KS channel function induced by an LQT5 mutation and other IsK mutants. *EMBO Journal*. **18**:4137-4148.

Ackerman MJ, Priori SG, Willems S, Berul C, Brugada R, Calkins H, Camm AJ, Ellinor PT, Gollob M, Hamilton R, Hershberger RE, Judge DP, Le Marec H, McKenna WJ, Schulze-Bahr E, Semsarian C, Towbin JA, Watkins H, Wilde A, Wolpert C, and Zipes DP (2011) HRS/EHRA expert consensus statement on the state of genetic testing for the channelopathies and cardiomyopathies: this document was developed as a partnership between the Heart Rhythm Society (HRS) and the European Heart Rhythm Association (EHRA). *Europace.* **13**:1077-1109.

Barhanin J, Lesage F, Guillemare E, Fink M, Lazdunski M, and Romey G (1996) K v LQT1 and IsK (minK) proteins associate to form the I Ks cardiac potassium current. *Nature*. **384**:78-80.

Bendahhou S, Marionneau C, Haurogne K, Larroque MM, Derand R, Szuts V, Escande D, Demolombe S, and Barhanin J (2005) In vitro molecular interactions and distribution of KCNE family with KCNQ1 in the human heart. *Cardiovascular Research*. **67**:529-538.

Bianchi L, Priori SG, Napolitano C, Surewicz KA, Dennis AT, Memmi M, Schwartz PJ, and Brown AM (2000) Mechanisms of I Ks suppression in LQT1 mutants. *American Journal of Physiology: Heart and Circulatory Physiology*. **279**:H3003-H3011.

Bollmann E, Schreiber JA, Ritter N, Peischard S, Ho HT, Wunsch B, Strunker T, Meuth S, Budde T, Strutz-Seebohm N, and Seebohm G (2020) 4,4'-Diisothiocyanato-2,2'-Stilbenedisulfonic Acid (DIDS) Modulates the Activity of KCNQ1/KCNE1 Channels by an Interaction with the Central Pore Region. *Cell Physiol Biochem*. **54**:321-332.

Bottegoni G, Kufareva I, Totrov M, and Abagyan R (2009) Four-dimensional docking: a fast and accurate account of discrete receptor flexibility in ligand docking. *Journal of medicinal chemistry*. **52**:397-406.

Busch AE, Herzer T, Wagner CA, Schmidt F, Raber G, Waldegger S, and Lang F (1994) Positive regulation by chloride channel blockers of I sK channels expressed in Xenopus oocytes. *Mol.Pharmacol.* **46**:750-753.

Campbell CM, Campbell JD, Thompson CH, Galimberti ES, Darbar D, Vanoye CG, and George AL, Jr. (2013) Selective targeting of gain-of-function KCNQ1 mutations predisposing to atrial fibrillation. *Circ Arrhythm Electrophysiol*. **6**:960-966.

Case DA, Cheatham TE, 3rd, Darden T, Gohlke H, Luo R, Merz KM, Jr., Onufriev A, Simmerling C, Wang B, and Woods RJ (2005) The Amber biomolecular simulation programs. *Journal of computational chemistry*. **26**:1668-1688.

Chen YH, Xu SJ, Bendahhou S, Wang XL, Wang Y, Xu WY, Jin HW, Sun H, Su XY, Zhuang QN, Yang YQ, Li YB, Liu Y, Xu HJ, Li XF, Ma N, Mou CP, Chen Z, Barhanin J, and Huang W (2003) KCNQ1 gain-of-function mutation in familial atrial fibrillation. *Science*. **299**:251-254.

Chung DY, Chan PJ, Bankston JR, Yang L, Liu G, Marx SO, Karlin A, and Kass RS (2009) Location of KCNE1 relative to KCNQ1 in the I(KS) potassium channel by disulfide cross-linking of substituted cysteines. *Proc.Natl.Acad.Sci.U.S.A*. **106**:743-748.

El Harchi A, Zhang H, and Hancox JC (2010) The S140G KCNQ1 atrial fibrillation mutation affects 'I(KS)' profile during both atrial and ventricular action potentials. *J Physiol Pharmacol*. **61**:759-764.

Eldstrom J, and Fedida D (2011) The voltage-gated channel accessory protein KCNE2: multiple ion channel partners, multiple ways to long QT syndrome. *Expert.Rev.Mol.Med.* **13**:e38.

Eldstrom J, McAfee DA, Dou Y, Wang Y, and Fedida D (2021) ML277 regulates KCNQ1 single-channel amplitudes and kinetics, modified by voltage sensor state. *J Gen Physiol*. **153**.

Gofman Y, Shats S, Attali B, Haliloglu T, and Ben-Tal N (2012) How does KCNE1 regulate the Kv7.1 potassium channel? Model-structure, mutations, and dynamics of the Kv7.1-KCNE1 complex. *Structure*. **20**:1343-1352.

690 Hedley PL, Jorgensen P, Schlamowitz S, Wangari R, Moolman-Smook J, Brink PA, Kanters JK, Corfield
691 VA, and Christiansen M (2009) The Genetic Basis of Long QT and Short QT Syndromes: A
692 Mutation Update. *Human Mutation*. **30**:1486-1511.
693 Hong K, Piper DR, Diaz-Valdecantos A, Brugada J, Oliva A, Burashnikov E, Santos-de-Soto J, Grueso-
694 Montero J, Diaz-Enfante E, Brugada P, Sachse F, Sanguinetti MC, and Brugada R (2005) De
695 novo KCNQ1 mutation responsible for atrial fibrillation and short QT syndrome in utero.
696 *Cardiovascular Research*. **68**:433-440.
697 Jakalian A, Jack DB, and Bayly CI (2002) Fast, efficient generation of high-quality atomic charges.
698 AM1-BCC model: II. Parameterization and validation. *Journal of computational chemistry*.
699 **23**:1623-1641.
700 Jervell A, and Lange-Nielsen F (1957) Congenital deaf-mutism, functional heart disease with
701 prolongation of the Q-T interval and sudden death. *Am Heart J*. **54**:59-68.
702 Kasuya G, and Nakajo K (2022) Optimized tight binding between the S1 segment and KCNE3 is required
703 for the constitutively open nature of the KCNQ1-KCNE3 channel complex. *Elife*. **11**.
704 Kuenze G, Vanoye CG, Desai RR, Adusumilli S, Brewer KR, Woods H, McDonald EF, Sanders CR,
705 George AL, Jr., and Meiler J (2020) Allosteric mechanism for KCNE1 modulation of KCNQ1
706 potassium channel activation. *Elife*. **9**.
707 Kvist T, Hansen KB, and Brauner-Osborne H (2011) The use of Xenopus oocytes in drug screening.
708 *Expert Opin Drug Discov*. **6**:141-153.
709 Lange A, Giller K, Hornig S, Martin-Eauclaire MF, Pongs O, Becker S, and Baldus M (2006) Toxin-
710 induced conformational changes in a potassium channel revealed by solid-state NMR. *Nature*.
711 **440**:959-962.
712 Lee SY, Banerjee A, and MacKinnon R (2009) Two separate interfaces between the voltage sensor and
713 pore are required for the function of voltage-dependent K(+) channels. *PLoS.Biol.* **7**:e47.
714 Magyar J, Horvath B, Banyasz T, Szentandrassy N, Birinyi P, Varro A, Szakonyi Z, Fulop F, and Nanasi
715 PP (2006) L-364,373 fails to activate the slow delayed rectifier K+ current in canine ventricular
716 cardiomyocytes. *Naunyn Schmiedebergs Arch Pharmacol*. **373**:85-89.
717 Maier JA, Martinez C, Kasavajhala K, Wickstrom L, Hauser KE, and Simmerling C (2015) ff14SB:
718 Improving the Accuracy of Protein Side Chain and Backbone Parameters from ff99SB. *Journal of*
719 *chemical theory and computation*. **11**:3696-3713.
720 Mattmann ME, Yu H, Lin Z, Xu K, Huang X, Long S, Wu M, McManus OB, Engers DW, Le UM, Li M,
721 Lindsley CW, and Hopkins CR (2012) Identification of (R)-N-(4-(4-methoxyphenyl)thiazol-2-
722 yl)-1-tosylpiperidine-2-carboxamide, ML277, as a novel, potent and selective K(v)7.1 (KCNQ1)
723 potassium channel activator. *Bioorg Med Chem Lett*. **22**:5936-5941.
724 Miller BR, 3rd, McGee TD, Jr., Swails JM, Homeyer N, Gohlke H, and Roitberg AE (2012)
725 MMPBSA.py: An Efficient Program for End-State Free Energy Calculations. *Journal of chemical*
726 *theory and computation*. **8**:3314-3321.
727 Mruk K, and Kobertz WR (2009) Discovery of a novel activator of KCNQ1-KCNE1 K channel
728 complexes. *PLoS One*. **4**:e4236.
729 Murray CI, Westhoff M, Eldstrom J, Thompson E, Emes R, and Fedida D (2016) Unnatural amino acid
730 photo-crosslinking of the channel complex demonstrates a KCNE1:KCNQ1 stoichiometry of up
731 to 4:4. *Elife.* **5**.
732 Neves MA, Totrov M, and Abagyan R (2012) Docking and scoring with ICM: the benchmarking results
733 and strategies for improvement. *Journal of computer-aided molecular design*. **26**:675-686.
734 Olesen MS, Nielsen MW, Haunso S, and Svendsen JH (2014) Atrial fibrillation: the role of common and
735 rare genetic variants. *Eur J Hum Genet*. **22**:297-306.
736 Oliver DS, Cunha LB, and Reynolds AC (1997) Markov chain Monte Carlo methods for conditioning a
737 permeability field to pressure data. *Mathematical Geology*. **29**:61–91.
738 Peng G, Barro-Soria R, Sampson KJ, Larsson HP, and Kass RS (2017) Gating mechanisms underlying
739 deactivation slowing by two KCNQ1 atrial fibrillation mutations. *Sci Rep*. **7**:45911.

740 Sanguinetti MC, Curran ME, Zou A, Shen J, Spector PS, Atkinson DL, and Keating MT (1996)
741 Coassembly of K v LQT1 and minK (IsK) proteins to form cardiac I Ks potassium channel.
742 *Nature*. **384**:80-83.
743 Smith JA, Vanoye CG, George AL, Jr., Meiler J, and Sanders CR (2007) Structural models for the
744 KCNQ1 voltage-gated potassium channel. *Biochemistry*. **46**:14141-14152.
745 Sun J, and MacKinnon R (2020) Structural Basis of Human KCNQ1 Modulation and Gating. *Cell*.
746 **180**:340-347 e349.
747 Toyoda F, Ueyama H, Ding WG, and Matsuura H (2006) Modulation of functional properties of KCNQ1
748 channel by association of KCNE1 and KCNE2. *Biochemical and Biophysical Research*
749 *Communications.* **344**:814-820.
750 Unsöld B, Kerst G, Brousos H, HÅbner M, Schreiber R, Nitschke R, Greger R, and Bleich M (2000)
751 KCNE1 reverses the response of the human K + channel KCNQ1 to cytosolic pH changes and
752 alters its pharmacology and sensitivity to temperature. *Pflugers Archiv European Journal of*
753 *Physiology*. **441**:368-378.
754 Wang Q, Curran ME, Splawski I, Burn TC, Millholland JM, VanRaay TJ, Shen J, Timothy KW, Vincent
755 GM, De Jager T, Schwartz PJ, Toubin JA, Moss AJ, Atkinson DL, Landes GM, Connors TD, and
756 Keating MT (1996) Positional cloning of a novel potassium channel gene: KVLQT1 mutations
757 cause cardiac arrhythmias. *Nat.Genet.* **12**:17-23.
758 Wang Y, Eldstrom J, and Fedida D (2020) The I Ks Ion Channel Activator Mefenamic Acid Requires
759 KCNE1 and Modulates Channel Gating in a Subunit-Dependent Manner. *Mol Pharmacol*.
760 **97**:132-144.
761 Wang Y, Zhang M, Xu Y, Jiang M, Zankov DP, Cui M, and Tseng GN (2012) Probing the structural
762 basis for differential KCNQ1 modulation by KCNE1 and KCNE2. *J.Gen.Physiol*. **140**:653-669.
763 Wang YH, Jiang M, Xu XL, Hsu KL, Zhang M, and Tseng GN (2011) Gating-related molecular motions
764 in the extracellular domain of the IKs channel: implications for IKs channelopathy. *J Membr Biol*.
765 **239**:137-156.
766 Westhoff M, Eldstrom J, Murray CI, Thompson E, and Fedida D (2019) I Ks ion-channel pore
767 conductance can result from individual voltage sensor movements. *Proc Natl Acad Sci U S A*.
768 **116**:7879-7888.
769 Willegems K, Eldstrom J, Kyriakis E, Ataei F, Dou Y, Russo S, Van Petegem F, and Fedida D (2022)
770 Structural and electrophysiological basis for the modulation of KCNQ1 channel currents by
771 ML277. *Nature Communications*. **13**.
772 Wu X, Brooks BR, and Vanden-Eijnden E (2016) Self-guided Langevin dynamics via generalized
773 Langevin equation. *Journal of computational chemistry*. **37**:595-601.
774 Xu X, Jiang M, Hsu KL, Zhang M, and Tseng GN (2008) KCNQ1 and KCNE1 in the IKs channel
775 complex make state-dependent contacts in their extracellular domains. *J.Gen.Physiol*. **131**:589-
776 603.
777 Xu Y, Wang Y, Zhang M, Jiang M, Rosenhouse-Dantsker A, Wassenaar T, and Tseng GN (2015)
778 Probing binding sites and mechanisms of action of an I(Ks) activator by computations and
779 experiments. *Biophys J*. **108**:62-75.
780 Yu H, Lin Z, Mattmann ME, Zou B, Terrenoire C, Zhang H, Wu M, McManus OB, Kass RS, Lindsley
781 CW, Hopkins CR, and Li M (2013) Dynamic subunit stoichiometry confers a progressive
782 continuum of pharmacological sensitivity by KCNQ potassium channels.
783 *Proc.Natl.Acad.Sci.U.S.A*. **110**:8732-8737.
784 Zachariae U, Schneider R, Velisetty P, Lange A, Seeliger D, Wacker SJ, Karimi-Nejad Y, Vriend G,
785 Becker S, Pongs O, Baldus M, and de Groot BL (2008) The molecular mechanism of toxin-
786 induced conformational changes in a potassium channel: relation to C-type inactivation.
787 *Structure*. **16**:747-754.
788 Zheng Y, Zhu X, Zhou P, Lan X, Xu H, Li M, and Gao Z (2012) Hexachlorophene is a potent
789 KCNQ1/KCNE1 potassium channel activator which rescues LQTs mutants. *PLoS One*. **7**:e51820.

Footnotes

This research was funded by Natural Sciences and Engineering Research Council of Canada (grant #RGPIN-2016-05422), Canadian Institutes of Health Research (#PJT-156181) and Heart and Stroke Foundation of Canada (#G17-0018392) grants to D.F. and grants from the Volkswagen Foundation (#AZ86659 and AZ 92111) to V.V.. MC holds an NSERC CGS-M scholarship. Y.W. holds a CIHR– Vanier CGS scholarship.

800
801 **Table 1.** Mean $V_{1/2}$ of activation (mV) and slope values (*k*-factor, mV) in the absence and presence
802 of mefenamic acid for fully saturated I_{Ks} channel complexes. A statistical difference in $V_{1/2}$
803 compared to control is shown as p-value, determined using an unpaired t-test. NS denotes not
804 significant. SEM is denoted by ±.
805

	Control			**100 µM or 1 mM Mefenamic Acid ***			**p-value**
	$V_{1/2}$	***k-factor***	**n**	**$V_{1/2}$**	***k-factor***	**n**	
Wildtype EQ	25.4 ± 2.4	19.4 ± 1.2	6	-80.3 ± 4.1	41.3 ± 8.4	3	<0.0001
K41C-EQ	15.2 ± 1.1	18.4 ± 1.7	4	11.4 ± 1.0	19.4 ± 0.8	4	<0.05
				16.7 ± 2.0	19.8 ± 1.4	3	NS
L42C-EQ	68.9 ± 1.5	21.5 ± 3.7	3	31.8 ± 0.4	14.8 ± 4.27	3	<0.01
E43C-EQ	70.8 ± 1.8	27.0 ± 2.8	4	46.4±2.1	29.1 ± 1.7	4	<0.01
A44C-EQ	4.1 ± 1.8	17.6 ±1.4	4	-5.6 ± 2.7	18.3 ± 2.0	4	<0.05
Y46A-EQ**	76.4 ± 1.5	57.3 ± 1.6	3	-29.8 ± 4.1	18.9 ± 3.1	3	<0.05
EQ-W323A	47.8 ± 2.7	23.7 ± 2.2	4	33.7 ± 1.2	28.5 ± 3.1	3	<0.05
EQ-W323C	54.0 ± 2.1	22.2 ± 2.1	4	27.5 ± 3.3	25.6 ± 1.8	4	<0.05
EQ-V324A	34.4 ± 2.3	20.7 ± 1.1	6	15.5 ± 2.3	27.9 ± 1.6	5	<0.05
EQ-V324W	41.0 ± 2.4	18.4 ± 0.3	4	27.3 ±6.0	25.5 ± 1.3	4	NS
EQ-Q147C	63.9 ± 5.8	25.4 ± 2.0	4	26.3 ± 5.7	32.7 ± 1.7	4	<0.05
EQ-Y148C	36.8 ± 0.3	20.3 ± 0.4	4	17.5 ± 4.0	36.7 ± 3.7	4	<0.05

806
807 * For K41C-EQ, the concentration of mefenamic acid used was either 100 µM (upper row values)
808 or 1 mM (lower row values). For all other constructs, 100 µM mefenamic acid was used.
809 ** An estimation of the activation $V_{1/2}$ was calculated from a right shifted, non-saturating GV
810 curve.

811 **Table 2.** Mean $V_{1/2}$ of activation (mV) and slope values (*k*-factor, mV) for WT EQ treated with
812 100 µM mefenamic acid, and untreated mutant EQ-L142C. Interpulse interval used is as indicated.
813 SEM is denoted by ±. An interpulse interval of 7 s created such a dramatic change in the shape of
814 the EQ-L142C G-V plot (see Figure 3- figure supplement 1) that a Boltzmann curve could not be
815 fit and $V_{1/2}$ and *k*-values are therefore not available.
816

	$V_{1/2}$	***k-factor***	**n**
WT EQ + 100 µM mefenamic acid: Interpulse interval 15 s	-80.3 ± 4.1	41.3 ± 8.4	3
WT EQ + 100 µM mefenamic acid: Interpulse interval 30 s	26.7 ± 10.5	66.6 ± 28	8
EQ-L142C control: Interpulse interval 15 s	-80.3 ± 4.5	30.0 ± 2.9	6
EQ-L142C control: Interpulse interval 30 s	-28.7 ± 19	62.5 ± 9.6	3

817
818

819 **Table 3.** Average free interaction energies of MEF-bound ps-I_{Ks} complexes calculated according
820 to MM/GBSA methods from three independent MD simulation runs. Mean values are in kcal/mol,
821 ± SD. For W323A and K41C mutations, calculations correspond to interval of simulations before
822 the detachment of ligand from molecular complex. Note that unbinding occurred in K41C and
823 W323A in all 3 simulations, e.g. Supplemental movies S2 and S3.
824

825

Run	Method	Wild Type	W323A	Y46C	K41C
I	**GBSA**	-39.3 ± 4.1 -	-13.0 ± 5.1 Unbinding after ~75 ns	-31.2 ± 2.9 -	-10.5 ± 3.8 Unbinding after ~25 ns
II	**GBSA**	-39.0 ± 3.3 -	-23.1 ± 3.1 Unbinding after ~120 ns	-32.2 ± 3.8 -	-17.0 ± 2.6 Unbinding after ~70 ns
III	**GBSA**	-35.5 ± 2.6 -	-22.6 ± 4.1 Unbinding after ~85 ns	-28.8 ± 5.7 -	-17.2 ± 2.5 Unbinding after ~20 ns

826 **Table 4.** Mean $V_{1/2}$ of activation (mV) and slope values (*k*-factor, mV) in the absence and presence
827 of 100 μM DIDS for fully saturated I_{Ks} channel complexes. A statistical difference in $V_{1/2}$
828 compared to control is shown as p-value determined using an unpaired t-test. NS denotes not
829 significant. SEM is denoted by ±
830

	Control			**100 μM DIDS**			**p-value**
	$V_{1/2}$	***k-factor***	**n**	**$V_{1/2}$**	***k-factor***	**n**	
Wildtype EQ	30.5 ± 4.3	20.3 ± 0.9	8	-16.1 ± 2.8	25.3 ± 1.9	5	<0.001
K41C-EQ	23.1 ± 3.0	20.2 ± 1.8	3	-1.6 ± 3.7	24.0 ± 3.6	3	<0.01
L42C-EQ	55.4 ± 3.3	19.9 ± 1.5	3	21.4 ±10.7	28.5 ± 2.6	4	<0.05
A44C-EQ	24.1 ± 1.7	29.6 ± 3.3	4	5.6 ± 2.4	17.6 ± 1.8	3	<0.05
***Y46A-EQ**	75.2 ± 2.1	59.1 ± 5.3	5	25.8 ± 0.9	39.2 ± 1.4	5	<0.0001
EQ-Y148C	51.8±4.6	23.5±1.7	4	40.0 ± 3.1	26.3 ± 1.5	5	**NS**
EQ-W323A	50.7 ± 3.6	23.9 ± 1.6	4	23.4 ± 4.9	24.1 ± 1.3	4	<0.05

831 * An estimation of the activation $V_{1/2}$ was calculated from a right shifted, non-saturating GV
832 curve.

833 **Table 5.** Average free interaction energies of DIDS-bound ps-I_{Ks} complexes calculated according
834 to MM/PBSA and MM/GBSA methods from three independent MD simulation runs. Mean values
835 are in kcal/mol, ± SD. For W323A and Y46C mutations, calculations correspond to interval of
836 simulations before the detachment of ligand from molecular complex. Note that unbinding
837 occurred in W323A in 2 of 3 simulations, and K41C did not unbind but the binding pose shifted –
838 see Supplemental movie S6.
839

Run	Method	Wild Type	W323A	Y46C	K41C	A44C	Y148C
I	**PBSA**	-32.3 ± 6.7	-25.7 ± 4.9	-35.5 ± 6.3	-33.5 ± 4.4	-29.2 ± 4.2	-34.1± 4.6
	GBSA	-35.5 ± 4.6	-30.2 ± 4.5 unbinding after 240 ns	-42.7 ± 5.4	-41.5 ± 5.8 changed binding pose after ~140-150 ns	-36.8 ± 2.9	-40.7 ± 4.0
II	**PBSA**	-32.6 ± 4.8	-25.3 ± 5.5	-25.7 ± 6.5	-36.4 ± 4.2	-29.0 ± 4.0	-29.3 ± 3.7
	GBSA	-36.0 ± 4.8	-30.0± 4.8	-32.4 ± 6.4 unbinding after ~100-132 ns	-31.6 ± 4.0	-34.0 ± 5.7	-31.8 ± 4.7
III	**PBSA**	-29.2 ± 8.1	-27.1± 3.9	-38.3 ± 4.8	-35.1 ± 4.3	-31.2 ± 45.0	-35.7 ± 5.8
	GBSA	-34.0 ± 8.9	-35.1± 4.8 unbinding after ~240 ns	-42.5 ± 4.7	-30.8 ± 3.9	-35.6 ± 5.6	-40.3 ± 5.9

840

841

Table 6: Average free energy of mefenamic acid and DIDS bound WT and mutant ps-I_{Ks} complexes. Values are calculated according to the MM/GBSA method from three independent MD simulation runs and further broken down by residue and channel region. For K41C and W323C, calculations correspond to the interval of simulations before detachment of the ligand from the complex. Values are in kcal/mol. Mutated residues are in bold italics.

	Residue	WT MEF	K41C MEF	Y46C MEF	W232A MEF	WT DIDS	A44C DIDS	Y46C DIDS	Y148C DIDS	W323A DIDS
Total		-38.02	-16.39	-31.40	-20.31	-34.29	-35.40	-39.16	-37.60	-34.33
Drug		-19.69	-8.79	-15.25	-11.65	-17.42	-17.52	-21.21	-18.18	-19.17
Channel		-17.91	-6.52	-16.61	-7.55	-19.21	-18.40	-16.94	-19.21	-15.10
Ch+Drug		-37.60	-15.31	-31.86	-19.20	-36.63	-35.92	-38.15	-37.39	-34.27
Difference		-0.42	-1.08	0.46	-1.11	2.34	0.52	-1.01	-0.21	-0.06
E1/E3	**K41**	-1.548	***-0.349***	-1.411	-0.954	-0.639	-0.439	-1.148	-0.283	0.083
	L42	-0.970	-0.895	-0.943	-1.193	-1.061	-0.798	-0.165	-0.320	-0.587
	E43	-2.681	-0.472	-2.257	-0.309	-1.312	-0.660	-0.014	-2.264	-0.705
	A44	-1.906	-0.886	-2.035	-1.102	-1.778	***-2.062***	-1.027	-1.061	-1.780
	M45	-1.744	-0.163	-1.913	-0.064	-1.756	-2.154	-1.222	-2.810	-1.633
	Y46	-2.391	-0.121	***-2.702***	-0.083	-1.985	-1.797	***-1.245***	-2.377	-1.603
	I47	-0.771	-0.136	-0.412	-0.203	-2.036	-1.993	-1.004	-0.621	-1.528
	L48	-0.010	-0.003	-0.025	0.005	-0.045	-0.100	-0.233	-0.081	-0.035
Sum		**-12.02**	**-3.03**	**-11.70**	**-3.90**	**-10.61**	**-10.00**	**-6.06**	**-9.82**	**-7.79**
Pore	**T322**	-0.125	-0.047	-0.091	-0.968	-0.200	-0.213	-0.127	-0.152	-0.410
	W323	-2.159	-0.736	-2.226	***-0.932***	-3.312	-3.395	-2.279	-3.566	***-1.590***
	V324	-0.644	-0.037	-0.123	-0.047	-0.172	-0.210	-0.111	-2.016	-0.063
	G325	-0.038	-0.006	-0.006	0.017	-0.004	0.000	0.003	-0.048	0.032
	K326	-0.185	-0.015	-0.024	0.008	0.038	0.058	0.091	0.000	0.118
	T327	-0.130	-0.015	-0.020	0.027	-0.040	-0.022	-0.018	-1.298	-0.014
Sum		**-3.28**	**-0.86**	**-2.49**	**-1.89**	**-3.69**	**-3.78**	**-2.44**	**-7.08**	**-1.93**
S1	**V141**	-0.061	-0.014	-0.247	-0.006	-0.569	-0.411	-0.660	-0.076	-0.504
	L142	-0.861	-0.434	-1.052	-0.267	-1.525	-0.822	-1.285	-0.460	-1.036
	S143	-0.028	0.004	-0.014	-0.063	-0.008	-0.006	-0.104	0.026	-0.017
	T144	-0.091	-0.006	-0.242	-0.526	-0.015	-0.122	-0.982	-0.002	-0.001
	I145	0.004	0.005	0.002	0.009	0.003	-0.329	-0.067	-0.009	-0.001
	E146	0.000	0.048	0.056	0.114	0.028	-0.014	-1.601	0.113	0.013
	Q147	-0.230	-0.365	0.006	-0.244	0.012	-0.143	-1.061	-0.974	-0.054
	Y148	-0.565	-1.556	0.006	-0.128	-0.428	-0.336	0.002	***-0.022***	-0.223
Sum		**-1.83**	**-2.32**	**-1.49**	**-1.11**	**-2.50**	**-2.18**	**-5.76**	**-1.40**	**-1.82**
Turret	**G297**	-0.024	-0.001	-0.010	-0.027	0.016	-0.027	-0.089	-0.001	-0.076
	S298	-0.320	-0.163	-0.419	-0.427	-0.791	-0.848	-1.107	-0.216	-1.026
	Y299	-0.103	-0.046	-0.104	-0.052	-0.718	-0.598	-0.563	-0.167	-0.673
	A300	-0.618	-0.183	-0.636	-0.431	-1.130	-1.112	-0.751	-0.652	-1.093
	D301	0.311	0.075	0.248	0.299	0.231	0.172	-0.181	0.136	-0.683
	A302	-0.024	-0.003	-0.011	-0.007	-0.011	-0.020	0.009	-0.008	-0.015
Sum		**-0.78**	**-0.32**	**-0.93**	**-0.65**	**-2.40**	**-2.43**	**-2.68**	**-0.91**	**-3.57**

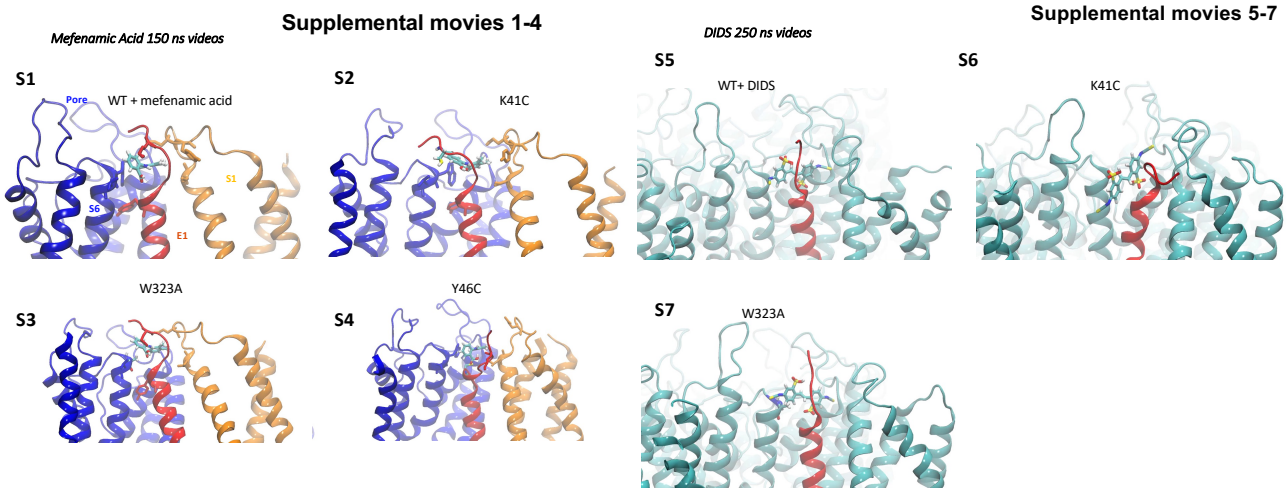

Supplemental movies 1-4. MD simulations at the molecular level of binding of mefenamic Acid to WT EQ, and K41C-EQ, W323A-EQ, Y46C-EQ mutants. Note that videos are longer than the actual simulations, durations stated below.

Movie S1. 80 ns simulation of mef binding to WT ps-KCNE1-KCNQ1.

Movie S2. 150 ns simulation of mef binding to K41C ps-KCNE1-KCNQ1

Movie S3. 110 ns simulation of mef binding to W323A ps-KCNE1-KCNQ1.

Movie S4. 120 ns simulation of mef binding to Y46C ps-KCNE1-KCNQ1

Supplemental movies 5-7. MD simulations at the molecular level of binding of DIDS to WT EQ, K41C-EQ, and W323A-EQ.

Movie S5. 220 ns simulation of DIDS binding to WT ps-KCNE1-KCNQ1.

Movie S6. 250 ns simulation of DIDS binding to K41C ps-KCNE1-KCNQ1

Movie S7. 250 ns simulation of DIDS binding to W323A ps-KCNE1-KCNQ1.

848